# Insights into methane dynamics from analysis of authigenic carbonates and chemosynthetic mussels at newly-discovered Atlantic Margin seeps

Prouty[1*], N.G., Sahy[2], D., Ruppel[3], C.D., Roark[4], E.B., Condon[2], D., Brooke[5], S., Ross[6], S.W. Demopoulos[7], A.W.J.

[1]US Geological Survey, Pacific Coastal and Marine Science Center, 400 Natural Bridges Drive Santa Cruz, CA 95060 nprouty@usgs.gov
[2]Department of Geography, Texas A&M University, College Station, TX 77843
[3] NERC Isotope Geosciences Laboratory, British Geological Survey, Nicker Hill, Keyworth NG12 5GG UK
[4] US Geological Survey, Woods Hole Coastal and Marine Science Center, Woods Hole, MA 02543
[5]Florida State University, Coastal and Marine Laboratory, 3618 Coastal Highway 98 St. Teresa, FL 32358
[6]University of North Carolina-Wilmington, Center for Marine Science, 5600 Marvin Moss Ln, Wilmington, NC 28409
[7]US Geological Survey, Wetland and Aquatic Research Center, 7920 NW 71st St., Gainesville, FL 32653
**corresponding author*

## Abstract

The recent discovery of active methane venting along the US northern and mid-Atlantic margin represents a new source of global methane not previously accounted for in carbon budgets from this region. However, uncertainty remains as to the origin and history of methane seepage along the tectonically inactive passive margin. Here we present the first isotopic analyses of authigenic carbonates and methanotrophic deep-sea mussels, *Bathymodiolus* sp., and the first direct constraints on the timing of past methane emission, based on samples collected at the upper slope Baltimore Canyon (~385 m water depth) and deepwater Norfolk (~1600 m) seep fields within the area of newly-discovered venting. The authigenic carbonates at both sites were dominated by aragonite, with an average $\delta^{13}C$ signature of -47‰, a value consistent with microbially driven anaerobic oxidation of methane-rich fluids occurring at or near the sediment-water interface. Authigenic carbonate U and Sr isotope data further support the inference of carbonate precipitation from seawater-derived fluids rather than from formation fluids from deep aquifers. Carbonate stable and radiocarbon ($\delta^{13}C$ and $\Delta^{14}C$) isotope values from living *Bathymodiolus* sp. specimens are lighter than those of seawater dissolved inorganic carbon, highlighting the influence of fossil carbon from methane on carbonate precipitation. U-Th dates on authigenic carbonates suggest seepage at Baltimore Canyon between 14.7±0.6 ka to 15.7±1.6 ka, and at the Norfolk seep field between 1.0±0.7 ka to 3.3±1.3 ka, providing constraint of the longevity of methane efflux at these sites. The age of the brecciated authigenic carbonates and the occurrence of pockmarks at the Baltimore Canyon upper slope could suggest a link between sediment delivery during Pleistocene sea-level lowstand, accumulation of pore fluid overpressure from sediment compaction, and release of overpressure through subsequent venting. Calculations show that the Baltimore Canyon site probably has not been within the gas hydrate stability zone (GHSZ) in the past 20 ka, meaning that in-situ release of methane from dissociating gas hydrate cannot be sustaining the seep. We cannot rule out updip migration of dissociating methane hydrate that occurs farther down the slope as a source of the venting at Baltimore Canyon, but consider that the history of rapid sediment accumulation and overpressure may play a more important role in methane emissions at this site.

Key words: authigenic carbonate; cold seep; AOM; chemosynthesis; mid-Atlantic margin; isotope geochemistry

## 1. Introduction

The distribution of newly discovered seafloor methane seeps along the US Atlantic margin (USAM) (Skarke et al., 2014) has important implications for ocean carbon dynamics (Boetius and Wenzhöfer 2013), continental slope stability and related hazards (Dugan and Flemings 2000; ten Brink et al. 2014), and also the geographic extent of chemosynthetic communities (Quattrini et al. 2015). Whereas seafloor methane venting typically occurs in major hydrocarbon basins such as the Gulf of Mexico or on active margins such as Cascadia, the northern USAM passive margin had long been considered relatively inactive (Skarke et al., 2014). Methane seeps have been documented on the southern USAM, at Cape Fear (L. Brothers et al. 2013) and Blake Ridge (Paull et al. 1995; Van Dover et al. 2003), where they occur at a depth range of 2155 to 2600 m above rising salt diapirs that perturb that gas hydrate stability field (Hornbach et al., 2005), but no such features were known on the northern part of the margin. This assessment was revised when geophysical surveys conducted between 2011 and 2013 identified ~570 gas plumes at water depths of 50-1700 m between Cape Hatteras and Georges Bank (Skarke et al. 2014). Observations at a few of the sites from remotely operated vehicles (ROV) included bubble streams, bacterial mats, chemosynthetic communities, authigenic carbonates, deep-sea corals, and gas hydrate (Skarke et al., 2014; Quattrini et al. 2015). Average contemporary methane emissions from seeps along the entire northern USAM are estimated at ~15 to 90 Mg $yr^{-1}$ (equivalent to 0.95 to 5.66 x $10^6$ mol $yr^{-1}$) based on analysis of ROV bubble observations (Skarke et al. 2014), versus 2.15 to 8.65 x $10^6$ mol $yr^{-1}$ in a seep field of Hudson Canyon based on the water column methane concentrations (Weinstein et al., 2016).

69 The origin and characteristics of the methane seeps north of Cape Hatteras remain elusive. No
70 underlying salt diapirs have been documented in the seeping areas, and Skarke et al. (2014)
71 postulate that dissociation of gas hydrate and possibly submarine groundwater discharge may
72 play a role in feeding seeps between the outer continental shelf and uppermost continental slope,
73 while the deeper seeps represent leakage of methane through fractured Eocene rocks.
74 Distinguishing among these and other processes that may be responsible for the methane
75 emissions requires direct study of seep fluids, rocks, and organisms. To acquire samples for such
76 studies, the Bureau of Ocean Energy Management (BOEM), the U.S. Geological Survey
77 (USGS), the National Oceanic and Atmospheric Administration (NOAA), and their academic
78 partners initiated a 5-year multi-disciplinary "Atlantic Deepwater Canyons" study focusing on
79 ecologically significant habitats (canyons, cold seeps, hard-bottoms and shipwrecks) in Norfolk
80 Canyon (off Virginia) and overlooking Baltimore Canyon (off Maryland) (Fig. 1). Of the two
81 sites, Baltimore Canyon had been previously investigated in the early 1980s with photographs of
82 a dense community of mussels at ~400 m obtained using a towed camera sled (B. Hecker, pers.
83 comm.), but no further work was conducted in the area until recently. During the Atlantic
84 Deepwater Canyons cruises, we used ROVs designed to support physical and biological
85 sampling to confirm the location of a shallow (~400 m) seep site overlooking Baltimore Canyon
86 in 2012 and, following the discovery of deep-sea gas plumes (NOAA, 2012), identified a new
87 chemosynthetic community at ~1600 m water depth south of Norfolk Canyon in 2013.
88
89 Authigenic carbonates are common at cold seeps and record a robust fingerprint of hydrocarbon
90 seep activity, including local and regional controls on the source and flux of carbon, the
91 conditions under which carbonates formed, and information regarding fluid-sediment and rock

92 interactions (see reviews in Campbell et al., 2006; Suess 2014). Additionally, authigenic
93 carbonates are amenable to uranium (U)-series dating techniques, and can provide key
94 information on the timing and duration of fluid venting at each seep (Teichert et al. 2003; Bayon
95 et al. 2009; Liebetrau et al., 2014). The isotopic composition of shells from chemosynthetic
96 bivalves living close to fluid vents represents an important archive of the nature and variability
97 of the venting. While previous studies have investigated authigenic carbonate formation and cold
98 seeps in other settings (Han et al., 2014; Suess 2014; Bayon et al., 2015) and fluid flow in
99 passive margins (Berndt 2005), this is the first study to examine the origin of the authigenic
100 carbonates, the source fluids, and the timing of methane emissions on the northern USAM. This
101 paper explores the geochemistry, mineralogy, and petrology of authigenic carbonates and bivalve
102 shells recovered by ROVs from both the Norfolk and the Baltimore Canyon seep fields with the
103 aim of tracing the origin and flow pathways of gas and fluids at both sites. Taken together, the
104 geochemical information derived from both authigenic carbonates and bivalve shells collected
105 from seeps in the Baltimore and Norfolk canyons expands our understanding of the origin and
106 occurrence of widespread methane seepage along the US Mid-Atlantic margin
107

108 **2. Methods**

109 2.1 Study site

110 A shallow (~385 m; Fig 2) seep site seaward and south of the location where Baltimore Canyon
111 (38° 03.086 N, 73° 49.379 W) crosses the shelf-break was surveyed and sampled during a 2012
112 cruise (17 Aug–14 Sep) aboard the NOAA ship *Nancy Foster* using the *Kraken II* ROV
113 (University of Connecticut). This site was sampled again in 2013, along with the deeper (1455-
114 1610 m; Fig. 3) Norfolk seep site (36° 51.921 N, 74° 29.574 W) during a cruise (2–18 May)

onboard the NOAA ship *Ronald H. Brown* using the *Jason II* ROV (Woods Hole Oceanographic Institution). At the Norfolk seep site, gas bubbles can be traced at least ~600 m above the seafloor (Fig. 3C), as confirmed by USGS surveys on the *R/V Endeavor* in April 2015 (Ruppel et al., 2015a). At the Baltimore Canyon seep field, water column imaging carried out by the USGS in April and September 2015 (Ruppel et al., 2015b) showed that venting is more widespread and diffuse (Fig. 2D). Dense colonies of chemosynthetic mussels, active gas bubbling, and extensive bacterial mats were observed at both seep sites (Fig. 2C and 3D) during the 2012 and 2013 ROV dives. Clams, common at the Blake Ridge seep site (Van Dover et al. 2003), were notably absent, as were tubeworms, a finding that is consistent with a recent survey of chemosynthetic communities from seep sites along the northeastern US continental margin (Quattrini et al., 2015). Seep communities at the Norfolk and Baltimore Canyon seep fields were dominated by the deep-sea mussels of the genus *Bathymodiolus*, which depends on chemosynthetic endosymbiotic bacteria to oxidize sulfur and/or methane for nutrition (Duperron et al. 2011).

2.2 X-Ray diffraction and petrography

Sample mineralogy was determined microscopically in thin sections, and by X-ray diffraction (XRD) using a Philips XRD with graphite monochromator at 40 kV and 45 mA. Step scans were run from 5° to 65° 2θ with 0.02° steps, using CuKα radiation and a count time of 2 s per step. XRD digital scan data were analyzed using the Philips X'Pert High Score search-and-match function to identify minerals. Mineral percentages were determined by multiplying unique peak intensities for each mineral in a sample by relative intensity factors. The products for all minerals in each sample were then summed to 100%. Carbonate content, reported as weight

137 percent (wt%), was determined using a coulometer at the USGS Pacific Coastal and Marine
138 Science Center, Santa Cruz, CA.
139
140 2.3 Stable isotopes
141 Stable carbon ($\delta^{13}C$) and oxygen ($\delta^{18}O$) isotopes were analyzed at the Stable Isotope
142 Geosciences Facility at Texas A&M University. Authigenic carbonate samples were subsampled
143 to isolate the cement and groundmass components. For the mussel shells, carbonate and
144 periostracum (organic rich outer layer) were collected along transects from the umbo to the
145 ventral margin of an individual specimen at discrete distances. Prior to analysis, the
146 periostracum material was acidified to remove inorganic carbon. Data were generated from a
147 Thermo-Finnigan MAT 253 with a Kiel IV Automated Carbonate Prep Device and are reported
148 in per mil (‰) relative to the international reference Pee Dee Belemnite (PDB). Analytical
149 uncertainties ($2\sigma$) of 0.04‰ for $\delta^{13}C$ and 0.06‰ for $\delta^{18}O$ are reported based on the long term
150 daily measurements of the international carbonate standard, NBS-19. Seawater samples were
151 measured for $\delta^{18}O$ using a Picarro L2120i cavity ringdown spectrometer at the Stable Isotope
152 Geoscience Facility at Texas A&M University, College Station. Isotope values were calibrated
153 to the VSMOW reference standard using internal reference standards JGULF and KONA. The
154 $\delta^{18}O$ value in VSMOW2 for JGULF is 1.22‰, and for Kona is -6.86‰. Average internal $\delta^{18}O$
155 precision is 0.12 ‰, and an external precision replicate of the same sample is 0.26‰.
156
157 Sulfur isotopes ($\delta^{34}S$) were determined at the Washington State University Stable Isotope Core
158 Laboratory. Mussel gill and seep sediment were combusted with an elemental analyzer (ECS
159 4010, Costech Analytical) coupled to a Delta PlusXP Thermo-Finnigan continuous flow isotope

ratio mass spectrometer. Sulfur isotope ratios ($\delta^{34}S$) are reported in per mil (‰) relative to VCDT (Vienna Canyon Diablo Troilite). Analytical accuracy (1σ) of $\delta^{34}S$ was determined by replicate analysis of internal lab standard referenced to IAEA standards, reported as 0.26‰ (n=36), bovine internal standard at 0.47‰ (n=18) and sample replicates 0.13‰ (n=9).

2.4 Strontium isotopes

The strontium isotope ($^{87}Sr/^{86}Sr$) compositions of the authigenic carbonates, mussel shells, and seawater samples were determined at the USGS facility at Menlo Park, California. Bottom water samples were filtered using a 0.45 μm glass fiber filter. Authigenic carbonate samples were subsampled to isolate the cement and groundmass components, and mussel shell material was homogenized using an agate mortar and pestle. The mussel shell and authigenic components were leached to remove labile Sr and digested in sealed Teflon vessels. Sr was separated from other ions using a Bio-Rad® AG-502-X8 cation exchange resin with HCl as the eluent. Purified Sr was converted to nitrate form, taken up in 30 μL of 0.15 M $H_3PO_4$ and loaded onto a Ta ribbon for mass spectrometric measurement. The isotopic composition was measured on a Finnigan MAT 261 multi-collector mass spectrometer using a static collection mode. All reported values of $^{87}Sr/^{86}Sr$ have been corrected for analytical fractionation to the standard $^{88}Sr/^{86}Sr$ ratio of 8.37521, and measurements are precise to ±0.00002 at the 95% confidence level.

2.5 Radiocarbon ($^{14}C$) analysis

Radiocarbon ($^{14}C$) analysis was performed on subsamples of authigenic carbonates and mussel shells collected from dead and live mussel specimens. Samples were prepared for Accelerator

Mass Spectrometry (AMS) radiocarbon ($^{14}C$) dating at the Keck Carbon Cycle AMS laboratory at UC Irvine (KCCAMS). Authigenic carbonate samples were subsampled to isolate the cement and groundmass components. Carbonate from the mussel shells was analyzed both as a homogenized powder as well as shell fragments. To test for potential contamination by secondary aragonite or calcite, duplicates were performed on samples treated with 10% HCl.

The carbonate samples were hydrolyzed to $CO_2$ in individual reaction chambers, evacuated, heated and acidified with orthophosphoric acid at 90°C. The resultant $CO_2$ was converted to graphite using an iron catalyst and the hydrogen reduction method (Vogel et al. 1987). Sample preparation backgrounds have been subtracted, based on measurements of $^{14}C$-free calcite and oxalic acid I. All $^{14}C$ results were corrected for isotopic fractionation according to the conventions of Stuiver and Polach (1977) with $\delta^{13}C$ values measured on prepared graphite using the AMS spectrometer. Radiocarbon concentrations are given as $\Delta^{14}C$ and conventional radiocarbon age following Stuiver and Polach (1977).

2.6 U-Th age dating of authigenic carbonates

U-Th dating of authigenic carbonates was carried out at the NERC Isotope Geosciences Laboratory, British Geological Survey. Samples were processed via total dissolution techniques, with isotope ratios measured on a Thermo Neptune Plus multi-collector ICP-MS, relative to a mixed $^{229}Th$-$^{236}U$ tracer calibrated against gravimetric solutions of CRM 112a U and Ames laboratory high purity Th. Details of the analytical protocol are provided in the Supplementary Material. U-Th age calculations were performed using an in-house Excel spreadsheet, and are calculated using the decay constants of Cheng et al. (2013).

206

207 **3. Results**

208 3.1 X-Ray diffraction and petrography

209 Calcium carbonate ($CaCO_3$) dominates the authigenic carbonate samples (48-97%) but not the
210 surrounding sediment (3-14%) (Table 1). Aragonite accounts for more than 60% of the
211 groundmass and up to 99% of the carbonate cement, with secondary amounts (< 15%) of low
212 and high-Mg calcite present, creating an aragonite-cemented intraclast breccia at both sites (Fig.
213 S1). The detrital fraction consists of poorly sorted accessory minerals, such as quartz, feldspar,
214 plagioclase, and pyroxene that are supported in a matrix of clay to silt-size particles, consistent
215 with grain size from the surrounding sediment. The clasts are sub-rounded to very angular,
216 particularly in the Baltimore Canyon specimen (Fig. 4). Voids between intraclasts and bivalve
217 shells are completely or partially filled with fibrous or bladed aragonite, showing multiple
218 generations of mineral growth. Fractures intersect well-developed radiating crystals of aragonite
219 in the Baltimore Canyon sample. Bioclasts are observed in both samples, either as intact shells,
220 aragonite filled, or skeletal molds. The organic carbon ($C_{org}$) content of the authigenic carbonate
221 groundmass and cement was less than 0.4%, whereas the sediment, especially at the Norfolk
222 seep site, had higher $\%C_{org}$ (Table 1). The shell carbonate was dominated by both aragonite
223 and/or calcite with $CaCO_3$ ranging between 95 to 97%.

224

225 3.2 Strontium isotopes

226 The strontium isotope ($^{87}Sr/^{86}Sr$) compositions of the authigenic carbonates and mussel shells
227 were investigated to constrain the fluid source and flow pathway for carbonate precipitation
228 (Sample et al., 1993). $^{87}Sr/^{86}Sr$ ratios for the authigenic carbonates, mussel shells, and water

samples ranged from 0.70915 to 0.70924 (Tables 1 and 2). The average authigenic carbonate (n=4) and mussel shell (n=2) $^{87}Sr/^{86}Sr$ ratios at both sites were equivalent, $0.70920 \pm 3x10^{-5}$ and $0.70920 \pm 2x10^{-5}$, respectively. In comparison, the average seawater (n=6) $^{87}Sr/^{86}Sr$ ratio was $0.70917 \pm 2x10^{-5}$ but was not statistically different (Student T-test; $p>0.05$) from the authigenic carbonate and shell samples.

3.3 Stable carbon, oxygen, and sulfur isotopes

At Norfolk, shells from both living and dead mussels yielded average $\delta^{13}C$ values of -2.59 ± 1.68‰ (n=34) and -7.10 ± 3.20‰ (n=16), respectively, and an average $\delta^{18}O$ value of 3.71 ± 0.25‰ (n=34) and 3.82 ± 0.39‰ (n=16), respectively (Table 2). No statistical difference (Student's t-test, $P>0.05$) exists between shell $\delta^{18}O$ values from dead and living specimens; however, shells from living mussels were significantly enriched in $^{13}C$ relative to shells from dead specimens (Student's t-test, $P<0.05$). Only shells from live mussel specimens were analyzed from the Baltimore Canyon seep site and yielded average shell $\delta^{13}C$ and $\delta^{18}O$ values of and -6.84 ± 1.97‰ and 2.57 ± 0.28‰ (n=30), respectively. At both sites, the shell $\delta^{13}C$ values were lighter relative to bottom water dissolved inorganic carbon (DIC) $\delta^{13}C$ values (0.90±0.05; n=2), but heavier relative to the Baltimore Canyon methane $\delta^{13}C$ value (-68‰; Pohlman et al., 2015). Compared to shells from Norfolk, mussel shell isotope values from Baltimore Canyon were heavier in $\delta^{13}C$ and $\delta^{18}O$ by ~4‰ and ~1‰, respectively. At both sites, shells $\delta^{18}O$ were enriched in $^{18}O$ relative to ambient seawater, where bottom water $\delta^{18}O$ values from Norfolk and Baltimore canyons were 0.34 and 0.53‰, respectively.

Shell isotopic variability over the lifespan of an individual specimen was calculated as the standard deviation of 8 to 12 stable isotope values from material collected along a transect from the umbo to the ventral margin (Fig. S2). Individual lifespan variability ranged from 0.11 to 0.56‰ and 0.69 to 3.57‰ for shell $\delta^{18}O$ and $\delta^{13}C$ values (n=13), respectively. On average, the $\delta^{18}O$ and $\delta^{13}C$ variability over the mussel lifespan was 0.24 and 1.49‰, respectively. Lifespan variability represented less than 10% of the average shell $\delta^{18}O$ signature at both sites, but up to 42% of the average shell $\delta^{13}C$ signal at the Norfolk seep site and 21% at the Baltimore Canyon seep site. The mussel periostracum $\delta^{13}C$ signature from samples collected at Norfolk seep field ranged from -70.66 to -29.92‰ (n=40), with an average value of -56.99±12.85‰ (Table 2). Mussel periostracum from Baltimore Canyon was not analyzed since sample preservation in ethyl alcohol precluded reliable $\delta^{13}C$ results.

The average $\delta^{13}C$ signature of the bulk authigenic carbonate from Norfolk and Baltimore canyons was -45.51±1.66‰ (n=5) and -48.43 ±1.02‰ (n=4), respectively. However, in comparison to the cement, the groundmass $\delta^{13}C$ values were heavier by 1-3‰ (Table 1). The bulk $\delta^{18}O$ values were similar, 3.80 ±0.05‰ (Norfolk, n=5) and 3.95±0.47‰ (Baltimore Canyon, n=4) with < 1‰ difference between the groundmass and cement at both sites (Table 1). The authigenic carbonate $\delta^{18}O$ values were heavier by ~3‰ relative to bottom water $\delta^{18}O$ values.

Sulfur ($\delta^{34}S$) isotopes were analyzed from *Bathymodiolus* sp. gill tissues collected at each seep field. Gill $\delta^{34}S$ values ranged from -4.07 to 21.55‰ (Table 3), with no statistical difference between the sites (Student's t-test, P>0.05); however, gill $\delta^{34}S$ values at Baltimore Canyon displayed a larger range compared to the Norfolk seep, from -4.07 to 18.13‰ (n=20) versus 8.65

to 21.55‰ (n=23). Periostracum $\delta^{34}S$ values from the Norfolk seep were similar to gill $\delta^{34}S$ values, ranging from 8.82 to 22.65‰, averaging 16.63±4.01‰ (n=28). Seep sediment $\delta^{34}S$ values averaged 5.53±2.16‰ (n=4) at Norfolk and 2.42±3.6‰ (n=5) at Baltimore Canyon (Table 3).

3.4 Radiocarbon ($^{14}C$) analysis

The $\Delta^{14}C$ signatures of the authigenic carbonates were significantly depleted in $^{14}C$, ranging from -959‰ to -740‰ with corresponding $^{14}C$ ages of 25,570±210 to 10,770±35 $^{14}C$ years (Table 4). The $^{14}C$ ages of mussel shells on the seabed were younger relative to the authigenic carbonate age. The $^{14}C$ age of the mussel shells derived from living specimens varied from 905±20 to 1,935±20 $^{14}C$ years, and the average $^{14}C$ age of the mussel shells derived from dead specimens at Norfolk was 1,345±20 $^{14}C$ years (Table 4). There was no statistical difference (Student's T-test, $P>0.05$) between shell from dead specimens that were pretreated with 10% HCl and those left untreated (Table 4), yielding an average $^{14}C$ age of 1,180 $^{14}C$ years, indicating that secondary aragonite and calcite are negligible.

3.5 U-Th age calculation

Discrete subsamples of late-stage cavity-filling authigenic carbonate weighing between 4.1-17.2 mg were hand-drilled from two hand specimens collected from the Baltimore (n=5) and Norfolk Canyon (n=5) sites (Fig. 4). These were analysed along with 9 detritus samples (5 from Norfolk and 4 from Baltimore Canyon) consisting of material loosely adhering to the outside surfaces of the hand specimens, and material recovered from the base of push cores collected within 2 km of the authigenic carbonates. Tabulated results are reported in Table 5. Authigenic carbonate

297 cement samples contained 3.2 to 4.6 ppm U, and 0.06 to 0.59 ppm Th. $^{230}Th/^{232}Th$ activity ratios
298 were between 2.2 and 8.6, clustering towards the lower end of the range reported from other
299 occurrences of methane-related authigenic carbonates (e.g., Teichert et al. 2003; Bayon et al.
300 2009; Fig. S3 A). The implication is that the analysed authigenic carbonates incorporate detrital
301 material, such as clay minerals, which carry $^{232}Th$, and an associated amount of initial $^{230}Th$.
302 Since initial $^{230}Th$ is not related to the in-situ decay of $^{234}U$, a correction is required in order to
303 calculate a robust carbonate precipitation age. The presence of initial $^{230}Th$ is typically
304 addressed via (i) leaching techniques aimed at separating the carbonate and detrital components
305 of a sample in order to calculate a two-point isochron age (e.g. Teichert et al., 2003; Berndt et al.,
306 2014), or total dissolution of the samples, with detrital corrections based on either (ii) a
307 theoretical detritus composition which assumes secular equilibrium in the $^{238}U$ decay chain, and
308 a $^{232}Th/^{238}U$ ratio linked to average continental crust composition (e.g. Aharon et al., 1997; Feng
309 et al., 2010; Liebetrau et al., 2014), or (iii) a measured, site-specific detrital isotopic composition
310 (e.g. Teichert et al., 2003; Bayon et al., 2009; 2015). Initial $^{230}Th$ in marine authigenic carbonates
311 is likely to be a mixture of $^{230}Th$ incorporated within the detrital material and hydrogenous $^{230}Th$
312 scavenged onto grain surfaces from the decay of $^{234}U$ in the water column, with the impact of the
313 latter increasing with water depth (Henderson and Anderson, 2003). Consequently, site-specific
314 corrections are likely to be more appropriate, particularly for samples collected at depths greater
315 than a few hundred meters. The impact of excess $^{230}Th$ scavenged from seawater is illustrated by
316 the measured ($^{230}Th/^{238}U$) of the five detritus samples from the Norfolk Canyon site (depth of
317 ~1600 m), which range from 1.7 to 2.1 (Table 5), and are significantly higher than the secular
318 equilibrium value of 1. Conversely ($^{230}Th/^{238}U$) values from the shallower Baltimore Canyon site
319 (depth ~385 m) are, as expected, lower (1.29-1.46) but still in excess of secular equilibrium.

Details of the average detrital U and Th compositions used to calculate corrected U-Th dates at Baltimore Canyon and Norfolk Canyon are provided in the supplementary material.

The U-Th ages from the Norfolk seeps, corrected for initial detrital and hydrogenous $^{230}$Th, range from 1.0±0.7 ka to 3.3±1.3 ka (Table 5). In comparison, the corrected U-Th ages of the Baltimore Canyon authigenic carbonate were older, ranging from 14.7±0.6 ka to 15.7±1.6 ka (Table 5). Modelled initial $(^{234}U/^{238}U)_i$ values are statistically equivalent to the mean modern seawater ($^{234}U/^{238}U$) of 1.1466 (Robinson et al., 2004; Fig. S3 B), meaning that U incorporated in the authigenic carbonates was sourced from seawater, rather than pore waters, which would be comparatively enriched in $^{234}$U (Henderson et al., 1999).

## 4. Discussion

### 4.1 Authigenic carbonate formation

The aragonite-dominated authigenic carbonates form pavements and/or irregular blocky build-ups on the seafloor. The carbonates consist of bioclasts, organic matter, and angular clasts of terrigenous origin. While the contemporary Baltimore Canyon does not connect with a river system, rivers delivered a significant volume of sediment to the submarine canyons incising the shelf during Pleistocene sea-level lowstands (e.g., Forde et al. 1981). The fluvial influence on the canyons is observed in both the geomorphic features and grain size, where coarse to medium grained, shelly terrigenous sands are observed adjacent to the canyon heads (Obelcz et al. 2014). The similarity between neodymium isotope ($^{143}Nd/^{144}Nd$) values from Baltimore Canyon surface sediment (0.51208; Prouty et al., 2015) and Hudson River sediment (0.51206; Goldstein and Jacobsen 1987) highlights past connectivity with proximal fluvial sources.

342 The authigenic carbonate texture may result from in-situ brecciation of weakly consolidated
343 sediment, possibly triggered by seismic and venting-induced disturbances, such as rapid
344 sedimentation related to episodic and rapid release of trapped fluids or gases (Matsumoto 1990).
345 Fractures cross cutting multiple generations of aragonite precipitate in the Baltimore Canyon
346 authigenic carbonate (Fig. 4) may signify past disturbance events. The dominance of aragonite
347 at both seep sites suggests precipitation at or close to the seafloor (see review in Suess 2014),
348 where sufficiently high sulfate concentrations inhibit high-Mg calcite crystallization (e.g.,
349 Bohrmann et al. 1998). This interpretation is consistent with carbonate $^{87}Sr/^{86}Sr$ and $\delta^{234}U$
350 isotope results that indicate precipitation from seawater-derived fluids (e.g., Naehr et al. 2007),
351 rather than deep-seated formation waters that are less radiogenic than modern seawater.
352
353 4.2 Anaerobic oxidation of methane
354 The main driver of authigenic carbonate precipitation at or near the sediment interface is
355 anaerobic oxidation of methane (AOM) via sulfate reduction ($CH_4 + SO_4^{2-} \rightarrow HCO_3^- + HS^- + H_2O$).
356 This reaction drives an increase in pore water alkalinity by the production of biocarbonate
357 ($HCO_3^-$) and favors carbonate precipitation. Carbonate precipitation from methanogenesis can
358 also occur deeper in the sediment column (e.g., Orphan et al. 2004; Gieskes et al. 2005) and is
359 typically characterized by carbonate $\delta^{13}C$ values > -40‰ (Aharon et al. 1997). However,
360 authigenic carbonate $\delta^{13}C$ values from Norfolk and Baltimore canyons are lighter (-45 to -48‰),
361 in agreement with $\delta^{13}C$ values at cold seep sites where microbial AOM is the dominant driver of
362 authigenic aragonite precipitation. The heavier $\delta^{13}C$ values of the authigenic carbonates
363 compared to methane represent the incorporation of seawater DIC that is relatively enriched in
364 $^{13}C$. Results of a two end-member $\delta^{13}C$ mixing model yield a contribution from methane-

365 derived carbon of ~70%, with the remaining ~30% attributed to seawater DIC-derived carbon
366 precipitated near the sediment-water interface. Furthermore, $\delta^{13}C$ values of AOM-related lipids
367 extracted from the authigenic carbonates were strongly depleted in $^{13}C$, (i.e., archaeol: -74.3‰;
368 Campbell et al., 2015), confirming the dominance of microbial methane as the dominant carbon
369 source for the Archaea. The authigenic carbonate $\delta^{13}C$ and $\delta^{18}O$ values are also consistent with
370 Group I carbonates that typify carbonate precipitation of microbial origin within the uppermost
371 few centimeters below the sediment-water interface (Joseph et al. 2013).
372
373 In addition to AOM, sulfate reduction is also a dominant process that occurs in methane-rich
374 sediments, resulting in sulfur fractionation in the pore water and sediment. Sulfate reduction
375 may therefore explain the light surface sediment $\delta^{34}S$ values (from -2.62 to 8.20‰; Table 3)
376 relative to seawater sulfate (+20‰; Heyl et al. 2007). The resulting hydrogen sulfide can then be
377 used to support the metabolic processes of surrounding chemosynthetic communities. For
378 example, Van Dover et al. (2003) reported that the mussel *B. heckerae* collected from Blake
379 Ridge derive up to 25% of their organic sulfur from sulfide. Using a two end-member mixing
380 model with a $H_2S$ $\delta^{34}S$ value of -10‰, and the average *Bathymodiolus* sp. gill $\delta^{34}S$ values from
381 each seep site, the reliance on $H_2S$ as an energy source at Norfolk and Baltimore canyon seep
382 fields was estimated at 16% and 14%, respectively. However, variable gill $\delta^{34}S$ values indicate
383 uptake of up to 80% of $H_2S$ (i.e., gill $\delta^{34}S$ value of -4.07‰ at the Baltimore Canyon Seep site),
384 suggesting free-living and/or symbiotic thiotrophic bacteria may play a nutritional role at the
385 base of the food web (Yamanaka et al. 2003). As an alternative to mussel tissue isotopic studies,
386 the mussel shell periostracum derived from both living and dead specimens represents a valuable
387 source of information about the seep environment. The similarity between the periostracum and

388 mussel gill $\delta^{34}S$ values from Norfolk suggests a high degree of nutrient flow between the soft
389 tissue, allowing for greater fidelity in using periostracum isotopic ratios in place of respirable
390 tissues of living specimens. This is particularly essential when mussel tissue is not available,
391 such as with archived specimens or those at quiescent vent sites.
392
393 4.3 Estimation of fluid composition and age
394 The composition of the seeping fluids can also be characterized by the mussel shell $\delta^{13}C$ values,
395 with differences between the living and dead specimens reflecting changes in the flux of methane
396 in the past, or possibly a change in the composition of the seeping fluids. At both sites, the shell
397 carbonate and periostracum $\delta^{13}C$ values were lighter relative to bottom water DIC $\delta^{13}C$ values
398 (Table 2). This difference suggests an additional carbon source for shell calcification, and
399 illustrates the decoupling between calcification and metabolic pathway (Aharon et al. 1997). The
400 light periostracum $\delta^{13}C$ values (-57‰; Table 2) agree with previous work concluding that mussel
401 shell periostracum originates from dietary sources, and is an alternative to soft tissue for trophic
402 studies (Geist et al. 2005). Assuming a regional methane $\delta^{13}C$ value of -68‰ (Pohlman et al.,
403 2015), the average percent contribution of methane to shell calcification was estimated at 11% at
404 Baltimore Canyon and 5% at Norfolk. However, shell $\delta^{13}C$ values from dead specimens
405 collected at Norfolk indicate a temporal shift in seepage activity and/or composition of seeping
406 fluids. Specifically, a reduction in $\delta^{13}C$ values of up to 17‰ observed in the dead specimens is
407 equivalent to a ~25% increase in methane contribution to shell calcification. Comparison of
408 relative $^{14}C$-derived ages from the dead and live specimens suggests this change could have
409 occurred within a few centuries (<500 years) (Table 4).
410

411 Carbonate shell $\delta^{13}C$ variability also has the potential to record environmental changes such as
412 changes in fluid source, as well as fluid-venting activity over the lifespan of the mussels (e.g.,
413 Lietard and Pierre 2008). Although the precise chronology of the variability is unknown because
414 of the difficulty in dating the specimens, estimates of ages of *B. brevior* and *B. thermophiles*
415 range from 18 to more than 25 years (Schöne and Giere 2005). Therefore**,** lifespan $\delta^{13}C$
416 variability reported above may be related to changes in methane flow within several decades.
417 The spatial distribution of living and dead mussels may also imply changing fluid composition or
418 flux rates, as suggested by Van Dover et al. (2003) from HOV dives on the Blake Ridge Diapir.
419
420 The shell carbonate $\delta^{18}O$ isotopic signature at Norfolk overlap with both *Bathymodiolus* and
421 *Calyptogena* shell samples from other cold seeps (Lietard and Pierre 2008). In comparison,
422 Baltimore Canyon shell $\delta^{18}O$ values are lighter, reflecting warmer in-situ temperatures (~9$^{o}$C)
423 relative to the deeper, colder in-situ temperatures (~4$^{o}$C) at Norfolk. Using bottom water $\delta^{18}O$
424 values from Baltimore and Norfolk canyons, the predicted carbonate $\delta^{18}O$ value precipitated at
425 equilibrium yields heavier carbonate $\delta^{18}O$ values relative to measured shell values from
426 Baltimore and Norfolk by 0.68 and 0.42‰ respectively. Therefore, there is evidence of isotopic
427 disequilibrium, indicating the influence of $^{18}O$-poor water and/or warmer seeping fluids (e.g.
428 Lietard and Pierre 2008). As a result, the predicted seawater temperatures using an aragonite
429 paleotemperature equation of Grossman and Ku (1986) are warmer by 1-3°C compared to
430 contemporary in-situ temperatures, a difference at least three times greater than the $\delta^{18}O$-derived
431 temperature analytical uncertainty of 0.28°C.
432

433 The influence of methane is also captured in the light carbonate $\Delta^{14}C$ values and relatively old
434 $^{14}C$-derived ages of mussel shells from living specimens. Seawater samples collected near the
435 Norfolk seep field yield an average $DI^{14}C$ value of -24.17±0.6‰, consistent with seawater $\Delta^{14}C$
436 values from below the mixed layer depth in Norfolk Canyon. In contrast, the average mussel
437 shell $\Delta^{14}C$ value from living specimens from the Norfolk seep field is -115±3‰. Assuming a
438 methane $\Delta^{14}C$ signature of -880‰ (<0.12 pMC; Pohlman et al. 2009) and a DIC $\Delta^{14}C$ signature
439 of -24‰ (this study), ~10% of the carbon signature for shell calcification is derived from fossil
440 carbon. As a result, the contribution from fossil carbon can yield a false $^{14}C$ carbonate age (e.g.,
441 Aharon et al. 1997). The dilution from fossil carbon may result in over prediction of $^{14}C$-derived
442 ages by 5 to 11%.
443
444 Owing to this incorporation of fossil carbon, we expect a disparity between the $^{14}C$-derived age
445 of the authigenic carbonates and the independently derived U-Th age. The average $\Delta^{14}C$
446 signatures of the authigenic carbonates at both sites are significantly depleted in $^{14}C$, with values
447 ranging from -894‰ to -878‰ and corresponding $^{14}C$ ages ranging from 17.99 to 19.35 ka. In
448 comparison, average U-Th ages from the Norfolk and Baltimore canyon seep sites were 1.0-3.3
449 ka and 14.7-15.7 ka, respectively. Thus, the disparity between the $^{14}C$ and U-Th derived ages is
450 a few thousand years at the Baltimore Canyon seep but at least 13 ka at the deepwater Norfolk
451 seep. The differences between the $^{14}C$ and U-Th ages are probably a complex function of
452 absolute age of the authigenic carbonates, methane flux, and the $^{14}C$ signature of the source
453 methane, and the results may imply greater incorporation of fossil carbon in the authigenic
454 carbonates at Norfolk Seep.
455

456 4.4 Formation model and paleoenvironment

457 The U-Th ages from methane derived authigenic carbonates indicate that hydrocarbon seepage
458 related to the formation of those carbonates occurred at the Baltimore Canyon seep field toward
459 the end of the Late Pleistocene, and was more recent (Holocene) at the Norfolk seep field. These
460 are the first absolute dates for the timing of hydrocarbon seepage along the US Atlantic margin,
461 and although the limited nature (single samples at two sites) these ages are supported by
462 additional U-Th dating conducted on more recently obtained authigenic carbonate samples along
463 the US Atlantic margin (Condon et al., 2015). Nonetheless, the origin of seeps and gas expulsion
464 geomorphic features (e.g., pockmarks and "gas blowouts") along the US Atlantic Margin
465 remains uncertain.

466

467 The occurrence of gas seeps and pockmarks associated with fluid expulsion at depths less than
468 500 m, which are outside the methane hydrate stability field, may have a microbial origin from
469 in-situ bacterial decay of organic matter or updip migration of gases produced by the same
470 process or released from methane hydrate dissociation at greater water depths on the upper slope
471 (Skarke et al. 2014). Such expulsion may also have a thermogenic origin at depth (Hill et al.
472 2004; Newman et al. 2008; Brothers et al. 2014). However, the geochemical analyses presented
473 here yield carbonate $\delta^{13}C$ values < -40‰. When coupled with observations by Pohlman et al.
474 (2015) of -68‰ in the bottom waters, a thermogenic origin for the methane is precluded. This
475 agrees with earlier work by Newman et al. (2008) that demonstrated the microbial origin of pore
476 fluid DIC $\delta^{13}C$ values along the US mid-Atlantic shelf break. Hill et al. (2004) argued that
477 microbial gas flowing updip from dissociating gas hydrates is responsible for the distribution of
478 gas blowouts in the region, and Skarke et al (2014) make the same argument for the distribution

479 of hundreds of seeps on the continental slope updip of the present-day hydrate stability limit,
480 particularly on the mid-Atlantic part of the margin. Recent multi-channel seismic profiles on the
481 upper continental slope below the Baltimore Canyon seep field do not reveal clear evidence for
482 strata that could be laterally channeling gas updip into the seeps (Ruppel et al., 2015b), but these
483 observations are equivocal.
484
485 An alternate explanation for the presence of the Baltimore Canyon seeps at ~400 m water depth
486 is that overpressures have accumulated within thick, rapidly deposited Pleistocene sediments,
487 leading to vertical fluid and gas expulsion (Brothers et al. 2014). Studies on passive margins
488 offshore Europe and Asia have also advanced this explanation for focused fluid flow in areas of
489 high sedimentation rates under excess pore pressure (Berndt 2005). This interpretation is
490 consistent with the non-aquifer model of Dugan and Flemings (2002), where rapid sediment
491 loading during the Pleistocene sea-level lowstand created overpressure gradients, forcing fluids
492 to migrate upward and outward toward the seafloor. During the Pleistocene, significant volumes
493 of sediment were delivered to the outer shelf, with much of it transported directly into shelf-
494 sourced canyons and then offshore to deep-sea fans (e.g., Poag 1992). The fluvial influence on
495 the canyons is observed in both the geomorphic features and grain size, where coarse to medium
496 grained, shelly terrigenous sands are observed adjacent to the canyon heads (Obelcz et al. 2014).
497 The Mid-Atlantic region is also marked by a seaward thickening wedge of shelf edge delta
498 deposits (200-400 m thick) (Hill et al., 2004; D. Brothers et al., 2013). Along the New Jersey
499 continental slope for example, sedimentation rates rose sharply during Pleistocene sea-level
500 lowstand (Dugan and Flemings, 2002), with rates as high as 353 cm $kyr^{-1}$ (McHugh and Olson,
501 2002). The age of the Baltimore Canyon authigenic carbonate further supports a link between

502 rapid loading by organic-rich sediment during the Pleistocene sea-level lowstand and subsequent
503 fluid flow from overpressure. Such overpressures may also contribute to pervasive slope
504 instability on this part of the Mid-Atlantic margin (ten Brink et al., 2014).
505
506 Our analysis (Fig. 5) shows that the Baltimore seep field would have been outside the methane
507 hydrate stability field even between 14.7±0.6 ka to 15.7±1.6 ka. The ensuing Late Pleistocene to
508 Holocene sea-level rise increased hydrostatic pressure, which could move the seep field closer to
509 the hydrate stability condition under isothermal conditions. However, dramatic bottom water
510 warming between the presumed cold Late Pleistocene temperature and the ~9°C observed in
511 2013 from in-situ temperature measurements overwhelms the impact of increased pressure. The
512 Baltimore Canyon seep field may now or in the past have emitted migrated methane that was
513 released by gas hydrate dissociation at greater water depths; however in-situ gas hydrate
514 dissociation is clearly ruled out as the source of methane emissions. This regime contrasts with
515 the hydrate-controlled methane venting off Svalbard, where seasonal fluctuations in bottom
516 water temperatures cause variable gas hydrate dissociation at a depth between 380 to 400 m
517 (Berndt et al., 2014).
518
519 The driving mechanism for methane venting the Norfolk seep field (~1600 m) is more difficult
520 to explain since the seep is well inside the gas hydrate stability zone and there is no underlying
521 salt diapir. Skarke et al. (2014) postulated that the Norfolk seep field is fed by gas flowing
522 through fractured Eocene rock, but a clear triggering mechanism that could explain seepage
523 consistent mid-Holocene U-Th date of the authigenic carbonates is lacking. Recent high-
524 resolution seismic imaging by the USGS shows fractures channeling methane to the seep sites

525 from hundreds of meters below the seafloor (Ruppel et al., 2015a). Despite the inferred deep
526 source of some of the methane, it is notable that the $\delta^{13}C$ data still support an entirely microbial
527 origin for the gas. There is evidence at both sites of upward flux of methane that is isotopically
528 similar between the sites with respect to carbon, most likely linked to long-term accumulation,
529 compaction, and over-pressuring of organic-rich sediment. This can occur when the intense
530 methane fluxes move the sulfate-methane transition zone (SMTZ) very close to the seafloor
531 (Orcutt et al., 2011).
532
533 4.5 Relationship to Global Setting
534 A variety of driving mechanisms has been proposed to explain methane venting at cold seeps,
535 including hydrological and tidal pumping, warming of bottom water (Suess 2014), excess pore
536 pressure in areas of high sedimentation along the passive margins of Europe and Africa (Berndt
537 2005), seismic activity (e.g., Fischer et al., 2013), and links to sea-level lowstands (e.g., Teichert
538 et al., 2003; Feng et al., 2010; Liebetrau et al., 2010). In many of these cases, a major mechanism
539 for methane release is a change in hydrostatic pressure and/or temperature, and subsequent
540 hydrate dissociation, as in the case of the South China Sea (Han et al., 2014) and Svalbard
541 (Westbrook et al., 2009; Berndt et al., 2014). Even with the assumption of very cold bottom
542 water temperatures, the Baltimore seep field would have been outside the methane hydrate
543 stability field at ~15ka (Fig. 5), meaning that in-situ gas hydrate dissociation cannot have ever
544 contributed to methane emissions there since the Late Pleistocene. Despite observations of
545 numerous landslide scars in the Baltimore Canyon landslide zone (ten Brink et al. 2014), ages
546 that could constrain the timing of slide events are are not available close to the seep site. The
547 ages farther downslope at the base of hemipelagic sediment overlying the youngest mass
548 transport deposit range between 5200 ± 150 and 10,080 yr BP (Embley, 1980). While these

549 dates are several thousand years younger than the age of the authigenic carbonate samples
550 analyzed from the Baltimore Canyon seep field site, the slide material that was dated is probably
551 not related to sediments originally at the top of the ridge where the seep field is located. For
552 now, we can only postulate that other passive margins with similar depositional regimes similar
553 to that of the northern US Atlantic margin may also be the loci of widespread and as-yet
554 undiscovered seepage that can be traced to similar mechanisms of overpressure accumulation
555 and eventual fluid expulsion, possibly with a slide-related connection.
556

557 **5. Conclusion**

558 The geochemistry, mineralogy, and petrology of authigenic carbonates and mussel shells
559 collected from two seep sites along the mid-Atlantic portion of the USAM in a newly-discovered
560 seep province provide the first direct information about methane sources, the processes driving
561 carbonate precipitation and chemosynthetic processes, and the nature of fluid-rock interaction.
562 Taken together, the $\delta^{234}U$, $^{87}Sr/^{86}Sr$, $\delta^{13}C$ and $\Delta^{14}C$ values support shallow precipitation of
563 aragonite driven by AOM and at equilibrium with seawater. At the deepwater Norfolk seep,
564 comparison of shell $\delta^{13}C$ values from dead and living specimens indicates a temporal shift in
565 seepage activity and/or composition of seeping fluids. Comparison between shell $\delta^{13}C$ values of
566 living versus dead specimens from Norfolk suggests a ~25% increase in methane contribution
567 within several centuries. In addition, changes in shell $\delta^{13}C$ values during growth may be related
568 to changes in methane flow throughout the organisms' lifespan (<25 years). The range of mussel
569 gill and periostracum $\delta^{34}S$ values from both sites suggests an admixture of sulfur sources,
570 hydrogen sulfide ($H_2S$) and seawater sulfate ($SO_4$), with the former sourced from sulfate
571 reduction during AOM. Lighter mussel shell $\Delta^{14}C$ values highlight dilution of the $^{14}C$ pool with

572 fossil carbon. As a result, authigenic carbonate $^{14}C$- and U-Th-derived ages are discordant.

573 According to U-Th ages, methane seepage is thought to have occurred at the uppermost slope
574 Baltimore Canyon seep field toward the end of the Pleistocene (14.7±0.6 ka to 15.7±1.6 ka) and
575 between 1.0±0.7 ka to 3.3±0.1.3 ka at the deepwater Norfolk seep field. Fluid flow from the
576 thick pile of overpressured Pleistocene sediments deposited at the sea-level lowstand is the most
577 likely mechanism to explain sustained methane venting at Baltimore Canyon, whereas venting
578 fluids at the Norfolk seeps, which are located well within the GHSZ, can be explained by flow
579 through fractured strata (Skarke et al. 2014; Ruppel et al., 2015a). At neither seep field does the
580 carbonate geochemistry support deep-sourced fluid of thermogenic origin. Instead, the isotope
581 and mineralogy of the carbonates indicate that microbial degradation of sedimentary organic
582 matter is the common source of widespread methane both outside (Baltimore Canyon) and well
583 within (Norfolk seep) the GHSZ. Results from this geochemical study, coupled with the
584 geophysical data of Skarke et al (2014) showing the distribution of seeps along the USAM,
585 highlights the potential role of the sedimentary framework in widespread venting at upper slope
586 locations updip of the current limit of gas hydrate stability. We postulate that high sedimentation
587 rate passive margins dominated by siliciclastic deposition due to glacial and fluvial processes
588 may have accumulated overpressures and produced episodes of fluid expulsion particularly
589 during Late Pleistocene lowstands. This implies that undiscovered methane seep provinces may
590 be widespread on upper continental slopes, which would have implications for carbon cycling
591 from the seafloor to overlying ocean-atmosphere system.

592 **Acknowledgments** Funding for this project (sponsored by the National Oceanographic
593 Partnership Program) included USGS Terrestrial, Freshwater, and Marine Environments
594 Program through the Outer Continental shelf study, Coastal and Marine Geology Program, and

595 the Bureau of Ocean Energy Management (BOEM) contract number M10PC00100 (contracted
596 to CSA Ocean Sciences, Inc.). C.R. was supported by USGS-DOE Interagency Agreements DE-
597 FE000291 and 0023495. We thank Greg Boland (BOEM) and Stephen Viada (CSA) for support
598 during the development of the overall project. We thank the crews of the NOAA ships *Nancy*
599 *Foster* and *Ronald H. Brown*, and *Kraken II* and *Jason II* ROVs, provided by the NOAA Office
600 of Ocean Exploration and Research. We thank D. Brothers, and J. Kluesner (USGS) for helpful
601 discussions, K. Davis (Texas A&M), B. Harlow (WSU), I. Aiello (MLML), S. Griffin (UCI),
602 and P. Campbell-Swarzenski, J. Fitzpatrick, and J. Hein (USGS) for analytical assistance, and J.
603 Bourque and J. McClain Counts (USGS) and M. Rhode (UNCW) for field and lab assistance. J.
604 Hein (USGS) and two anonymous reviewers provide valuable input. Any use of trade, product,
605 or firm names is for descriptive purposes only and does not imply endorsement by the U.S.
606 Government.

607

608

609 **Figure Captions**

610 **Figure 1**

611 Location map showing the Norfolk and Baltimore Canyon seep fields (green circles) relative to
612 the major shelf-break canyons (Norfolk, Washington, and Baltimore). The blue triangle outlines
613 the study area for the multi-disciplinary "Atlantic Deepwater Canyons" study.

614

615 **Figure 2**

616 (A) Baltimore Canyon, with the seep field located on the southern promontory overlooking the
617 canyon. The green circle denotes the seep that was sampled for mussel shells and authigenic

carbonates within the seep field. (B) Close-up view of shaded relief at the Baltimore Canyon seep field, with bathymetric contours at 100 m spacing. The green circle denotes the seep that is the focus of this paper. Red and orange circles are seeps from the Skarke et al. (2014) database and from USGS water-column imaging surveys in April 2015, respectively. Some of the orange and red seeps may correspond to the same location within the resolution of the data. Yellow symbols are pockmarks mapped by Brothers et al. (2014). (C) Left: In-situ photo of deep-sea mussel field of *Bathymodiolus* sp. Right: In-situ photo of deep-sea Cusk fish, *Brosme brosme*, beneath authigenic pavement in soft substrate with low live mussel cover (D) Target strength calculated from water column imagery collected with a Simrad EK60 using a 38 kHz transducer during USGS surveys across the seep field in September 2015. The current deflects the plumes slightly southeast in the water column. The analysis used the approach and software described in Veloso et al. (2015).

**Figure 3**.

(A) Norfolk deep seep field, showing the locations of seeps in the Skarke et al. (2014) database (red circles) and the sampled seep for authigenic carbonate and mussels as a green circle. (B) Close-up of the Norfolk seep field, using the same key as in (A). (C) NOAA image of the plumes emanating from the seep field in 2013, with the seep sampled for this paper indicated in yellow. (D) Left: In-situ photo of dense deep-sea mussel field of live *Bathymodiolus* sp. on irregular blocky build-up on the seafloor. Right: In-situ photos of live *Bathymodiolus* sp. at active seep site with visible bubble stream.

**Figure 4**

Photographic and petrographic thin section images (plane polarized light; 40x) of the authigenic carbonates sampled at the Norfolk seep site (dive NF-2012-14) and Baltimore Canyon seep site (dive RB-2013-682). Infilling of voids by acicular aragonite, detrital grains, organic matter, and bioclasts are noted in the matrix-supported clay to silt-size aragonite-dominated breccia. Locations of sampling sites for U-Th dates (red squares) and radiocarbon (yellow squares) are shown for their respective locations and corresponding sample number from Tables 4 and 5.

**Figure 5**

The evolution of Baltimore Canyon (squares) and Norfolk (circles) seeps in depth-temperature (P-T) space relative to the methane hydrate stability field calculated with seawater salinity. Closed symbols are present-day depth and temperature, and open symbols denote estimated conditions at 15.1±1.6 ka and 3±1 ka, respectively.

## References

Aharon P, Schwarcz HP, Roberts HH (1997) Radiometric dating of submarine hydrocarbon seeps in the Gulf of Mexico. Geol Soc Am Bull 109:568-579

Bayon G, Henderson GM, Bohn M (2009) U–Th stratigraphy of a cold seep carbonate crust. Chem Geol 260:47-56

Bayon G, Henderson GM, Etoubleau J, Caprais J-C, Ruffine L, Marsset T, Dennielou B, Cauquil E, Voisset M, Sultan N (2015) U-Th isotope constraints on gas hydrate and pockmark dynamics at the Niger delta margin. Mar Geol 370:87-98

Berndt C (2005) Focused fluid flow in passive continental margins. Phil. Trans. R. Soc. A s 363:2855-2871

Berndt C, Feseker T, Treude T, Krastel S, Liebetrau V, Niemann H, Bertics VJ, Dumke I, Dünnbier K, Ferré B, Graves C, Gross F, Hissmann K, Hühnerbach V, Krause S, Lieser K, Schauer J, Steinle L (2014) Temporal Constraints on Hydrate-Controlled Methane Seepage off Svalbard. Science 343:284-287

Boetius A, Wenzhöfer F (2013) Seafloor oxygen consumption fuelled by methane from cold seeps. Nature Geosci 6:725-734

Bohrmann G, Greinert J, Suess E, Torres M (1998) Authigenic carbonates from the Cascadia subduction zone and their relation to gas hydrate stability. Geology 26:647-650

Brothers LL, Van Dover CL, German CR, Kaiser CL, Yoerger DR, Ruppel CD, Lobecker E, Skarke AD, Wagner JKS (2013) Evidence for extensive methane venting on the southeastern U.S. Atlantic margin. Geology 41:807-810

Brothers DS, Luttrell KM, Chaytor JD (2013) Sea-level–induced seismicity and submarine landslide occurrence. Geology 41:979-982

675 Brothers DS, Ruppel C, Kluesner JW, Brink US, Chaytor JD, Hill JC, Andrews BD, Flores C (2014) Seabed fluid
676 expulsion along the upper slope and outer shelf of the US Atlantic continental margin. Geophys Res Lett 41:96-
677 101
678 Campbell KA (2006) Hydrocarbon seep and hydrothermal vent paleoenvironments and paleontology: Past
679 developments and future research directions. Palaeogeogr. Palaeoclimatol. Palaeoecol. 232:362-407
680 Campbell PL, Prouty NG, Demopoulos, AWD, Roark, EB, Coykendall (2015) Lipid biomarkers and their specific
681 carbon isotopic composition from cold seep community authigenic carbonates and sediments from the Mid-
682 Atlantic Norfolk and Baltimore Canyons. Fall Meeting Amer. Geophys. Union, OS33A-2015.
683 Cheng H, Lawrence Edwards R, Shen C-C, Polyak VJ, Asmerom Y, Woodhead J, Hellstrom J, Wang Y, Kong X,
684 Spötl C, Wang X, Calvin Alexander Jr E (2013) Improvements in $^{230}$Th dating, $^{230}$Th and $^{234}$U half-life values,
685 and U–Th isotopic measurements by multi-collector inductively coupled plasma mass spectrometry. Earth Planet
686 Sci Lett 371–372:82-91
687 Condon D, Sahy D, Ruppel C, Prouty N, Noble S, Team SP (2015) Tempo and longevity of methane efflux along
688 the US Atlantic margin. A Fall Meeting Amer. Geophys. Union, OS31B-07.
689 Dugan B, Flemings PB (2000) Overpressure and fluid flow in the New Jersey continental slope: implications for
690 slope failure and cold seeps. Science, 289, 288–9
691 Dugan B, Flemings PB (2002) Fluid flow and stability of the US continental slope offshore New Jersey from the
692 Pleistocene to the present. Geofluids 2:137-146
693 Duperron S, Guezi H, Gaudron SM, Pop Ristova P, Wenzhöfer F, Boetius A (2011) Relative abundances of
694 methane−and sulphur−oxidising symbionts in the gills of a cold seep mussel and link to their potential energy
695 sources. Geobiology 9:481-491
696 Embley RW (1980) The role of mass transport in the distribution and character of deep- ocean sediments with
697 special reference to the North Atlantic. Marine Geology 38, 23–50.
698 Feng D, Roberts HH, Cheng H, Peckmann J, Bohrmann G, Lawrence Edwards R, Chen D (2010) U/Th dating of
699 cold-seep carbonates: An initial comparison. Deep Sea Research Part II: Topical Studies in Oceanography
700 57:2055-2060
701 Fischer D, Mogollón JM, Strasser M, Pape T, Bohrmann G, Fekete N, Spiess V, Kasten S. (2013) Subduction zone
702 earthquake as potential trigger of submarine hydrocarbon seepage. Nature Geoscience. 1;6(8):647-51
703 .Forde EB, Stanley DJ, Sawyer WB, Slagle KJ (1981) Sediment transport in Washington and Norfolk submarine
704 canyons. Appl Ocean Res 3:59-62
705 Geist J, Auerswald K, Boom A (2005) Stable carbon isotopes in freshwater mussel shells: Environmental record or
706 marker for metabolic activity? Geochim Cosmochim Acta 69:3545-3554
707 Gieskes J, Mahn C, Day S, Martin JB, Greinert J, Rathburn T, McAdoo B (2005) A study of the chemistry of pore
708 fluids and authigenic carbonates in methane seep environments: Kodiak Trench, Hydrate Ridge, Monterey Bay,
709 and Eel River Basin. Chem Geol 220:329-345
710 Goldstein SJ, Jacobsen SB (1987) The Nd and Sr isotopic systematics of river-water dissolved material: implications
711 for the sources of Nd and Sr in seawater. Chem. Geol. (Isot. Geosci. Sect.) 66:245-272
712 Grossman E, Ku TL (1986) Oxygen and carbon isotope fractionation in biogenic aragonite: Temperature effects.
713 Isot Geosci 59:59-74
714 Han X, Suess E, Liebetrau V, Eisenhauer A, Huang Y (2014) Past methane release events and environmental
715 conditions at the upper continental slope of the South China Sea: constraints by seep carbonates. Int. J. Earth Sci.
716 103:1873-1887
717 Henderson GM, Anderson RF (2003) The U-series toolbox for paleoceanography. In Bourdon B, Henderson GM,
718 Lundstrom CC, Turner SP (eds) Uranium Series Geochemistry, Rev. Mineral. Geochem, 52:493-531
719 Henderson GM, Slowey NC, Haddad GA (1999) Fluid flow through carbonate platforms: constraints from
720 234U/238U and Cl- in Bahamas pore waters. Earth Planet. Sci. Lett. 169:99-111
721 Heyl TP, Gilhooly WP, Chambers RM, Gilchrist GW, Macko SA, Ruppel CD, Van Dover CL (2007)
722 Characteristics of vesicomyid clams and their environment at the Blake Ridge cold seep, South Carolina, USA.
723 Mar Ecol Prog Ser 339:169-184
724 Hill JC, Driscoll NW, Weissel JK, Goff JA (2004) Large−scale elongated gas blowouts along the US Atlantic
725 margin. J. Geophys. Res., 109, B09101, doi:10.1029/2004JB002969.
726 Holden NE (1990) Total half-lives for selected nuclides. Pure Appl Chem 62(5):941-958
727 Hornbach MJ, Ruppel C, Saffer DM, Van Dover CL, Holbrook WS (2005) Coupled geophysical constraints on heat
728 flow and fluid flux at a salt diapir. Geophys Res Lett 32(24) doi: 10.1029/2005GL024862

729 Jaffrey A, Flynn K, Glendenin L, Bentley W, Essling A (1971) Precision measurement of half-lives and specific
730 activities of $^{235}U$ and $^{238}U$, Phys. Rev. C, 4*(5),* 1889–1906,10.1103/PhysRevC.4.1889.
731 Joseph C, Campbell KA, Torres ME, Martin RA, Pohlman JW, Riedel M, Rose K (2013) Methane-derived
732 authigenic carbonates from modern and paleoseeps on the Cascadia margin: Mechanisms of formation and
733 diagenetic signals. Palaeogeogr. Palaeoclimatol. Palaeoecol. 390:52-67
734 Lietard C, Pierre C (2008) High-resolution isotopic records ($\delta^{18}O$ and $\delta^{13}C$) and cathodoluminescence study of
735 lucinid shells from methane seeps of the Eastern Mediterranean. Geo-Mar Lett:195-203
736 Liebetrau V, Augustin N, Kutterolf S, Schmidt M, Eisenhauer A, Garbe-Schönberg D, Weinrebe W (2014) Cold-
737 seep-driven carbonate deposits at the Central American forearc: contrasting evolution and timing in escarpment
738 and mound settings. Int. J. Earth Sci. 103:1845-1872
739 Matsumoto R (1990) Vuggy carbonate crust formed by hydrocarbon seepage on the continental shelf of Baffin
740 Island, northeast Canada. Geochem J 24:143-158
741 McHugh CMG, Olson HC (2002) Pleistocene chronology of continental margin sedimentation:: New insights into
742 traditional models, New Jersey. Mar Geol 186:389-411
743 Naehr TH, Eichhubl P, Orphan VJ, Hovland M, Paull CK, Ussler Iii W, Lorenson TD, Greene HG (2007)
744 Authigenic carbonate formation at hydrocarbon seeps in continental margin sediments: A comparative study.
745 Deep Sea Res II 54:1268-1291
746 Newman KR, Cormier M-H, Weissel JK, Driscoll NW, Kastner M, Solomon EA, Robertson G, Hill JC, Singh H,
747 Camilli R (2008) Active methane venting observed at giant pockmarks along the US mid-Atlantic shelf break.
748 Earth Planet Sci Lett 267:341-352
749 NOAA (2012) NOAA explorers discover deepwater gas seeps off U.S. Atlantic coast. Press Release
750 (http://www.noaanews.noaa.gov/stories2012/20121219_gas_seeps.html)
751 Obelcz J, Brothers D, Chaytor J, Brink Ut, Ross SW, Brooke S (2014) Geomorphic characterization of four shelf-
752 sourced submarine canyons along the U.S. Mid-Atlantic continental margin. Deep Sea Res II 104:106-119
753 Olsson, IU (1970) The use of Oxalic acid as a Standard. In I.U. Olsson, ed., Radiocarbon Variations and Absolute
754 Chronology, *Nobel Symposium, 12th Proc.,* John Wiley & Sons, New York, p. 17.
755 Orcutt BN, Sylvan JB, Knab NJ, Edwards KJ (2011) Microbial ecology of the dark ocean above, at, and below the
756 seafloor. Microbiol Mol Biol Rev 75:361-422
757 Orphan VJ, Ussler W, Naehr TH, House CH, Hinrichs KU, Paull CK (2004) Geological, geochemical, and
758 microbiological heterogeneity of the seafloor around methane vents in the Eel River Basin, offshore California.
759 Chem Geol 205:265-289
760 Paull CK, Ussler W, Borowski WS, Spiess FN (1995) Methane-rich plumes on the Carolina continental rise:
761 Associations with gas hydrates. Geology 23:89-92
762 Poag CW (1992) U.S. Middle Atlantic Continental Rise: Provenance, Dispersal, and Deposition of Jurassic to
763 Quaternary Sediments. In: Poag CW, Graciansky PC (eds) Geologic Evolution of Atlantic Continental Rises.
764 Van Nostrand Reinhold, New York, pp100-156
765 Pohlman JW, Kaneko M, Heuer VB, Coffin RB, Whiticar M (2009) Methane sources and production in the northern
766 Cascadia margin gas hydrate system. Earth Planet Sci Lett 287:504-512
767 Pohlman, J., C. Ruppel, R. Colwell, S. Krause, T. Treude, M. Graw, M. Casso, L.-G. Boze, B. Buczkowki, and D.
768 Brankovits, 2015, Sediment and water column chemistry related to methane seepage along the northern US
769 Atlantic margin, Fall Meeting Amer. Geophys. Union, OS33A-1992.
770 Prouty , NG, Swarzenski, Mienis, F., Davies, A.J., Demopoulos, A., Condon, D. Ross, S, and Brooke, S. (2015)
771 Sources of Organic Matter to Deep-sea Corals Living in Submarine Canyons of the Mid-Atlantic Bight Region,
772 U.S. Aquatic Sciences ASLO Meeting, 27449
773 Quattrini AM, Nizinski MS, Chaytor JD, Demopoulos AWD, Roark EB, France SC, Moore JA, Heyl TP, Auster PJ,
774 Kinlan B, Ruppel C, Elliott KP, Kennedy BRC, Lobecker E, Skarke A, Shank T (2015) Exploration of the
775 Canyon-Incised Continental Margin of the Northeastern United States Reveals Dynamic Habitats and Diverse
776 Communities. PLoS ONE 10(10): e0139904. doi:10.1371/journal.pone.0139904
777 Robinson FL, Belshaw NS, Henderson GM (2004) U and Th concentrations and isotope ratios in modern carbonates
778 and waters from the Bahamas. Geochim. Cosmochim. Acta. 68:1777-1789
779 Ruppel C, Kluesner JW, Danforth W (2015a) Imaging Methane Seeps and Plumes on the U.S. Atlantic Margin
780 Sound Waves March June 2015. U.S. Geological Survey http://soundwaves.usgs.gov/2015/06/fieldwork3.html
781 Ruppel, C, Kluesner, JW, Pohlman J, Brothers D, Colwell F, Krause S. and Treude T. (2015b) Methane Hydrate
782 Dynamics on the US Atlantic Margin. DOE Fire-in-the -Ice 15(2): 10-13.

783 Sample JC, Reid MR, Tobin HJ, Moore JC (1993) Carbonate cements indicate channeled fluid flow along a zone of
784 vertical faults at the deformation front of the Cascadia accretionary wedge (northwest U.S. coast). Geology
785 21:507-510
786 Schöne BR, Giere O (2005) Growth increment and stable isotope variation in shells of the deep-sea hydrothermal
787 vent bivalve mollusk *Bathymodiolus brevior* from the North Fiji Basin Pacific Ocean. Deep Sea Res I 52:1896–
788 1910
789 Skarke A, Ruppel C, Kodis M, Brothers D, Lobecker E (2014) Widespread methane leakage from the seafloor on
790 the northern US Atlantic margin. Nature Geosci 7:657-661
791 Stuiver M, Polach HA (1977) Discussion reporting of $^{14}C$ data. Radiocarbon 19:355-363
792 Suess E (2014) Marine cold seeps and their manifestations: geological control, biogeochemical criteria and
793 environmental conditions. Int. J. Earth Sci. 103:1889-1916
794 Teichert BMA, Eisenhauer A, Bohrmann G, Haase-Schramm A, Bock B, Linke P (2003) U/Th systematics and ages
795 of authigenic carbonates from Hydrate Ridge, Cascadia Margin: recorders of fluid flow variations. Geochim
796 Cosmochim Acta 67:3845-3857
797 ten Brink US, Chaytor JD, Geist EL, Brothers DS, Andrews BD (2014) Assessment of tsunami hazard to the U.S.
798 Atlantic margin. Mar Geol 353:31-54
799 Van Dover CL, Aharon P, Bernhard JM, Caylor E, Doerries M, Flickinger W, Gilhooly W, Goffredi SK, Knick KE,
800 Macko SA, Rapoport S, Raulfs EC, Ruppel C, Salerno JL, Seitz RD, Sen Gupta BK, Shank T, Turnipseed M,
801 Vrijenhoek R (2003) Blake Ridge methane seeps: characterization of a soft-sediment, chemosynthetically based
802 ecosystem. Deep Sea Res I 50:281-300
803 Veloso M, Greinert J, Mienert J, De Batist M (2015), A new methodology for quantifying bubble flow rates in deep
804 water using splitbeam echosounders: Examples from the Arctic offshore NW-Svalbard. Limnol Oceanogr:
805 Methods, 13: 267–287. doi: 10.1002/lom3.10024
806 Vogel JS, Southon JR, Nelson DE (1987) Catalyst and binder effects in the use of filamentous graphite for AMS.
807 Nucl. Instr. Meth. Phys. Res. 29:50-56
808 Weinstein A, Navarrete L, Leonte M, Weber T, Ruppel C, Kellermann M, Arrington E, Valentine DL, Chepigin A,
809 Rosemore B, Green A, Du M., Scranton MI, Kessler JD (2016) Determining the flux of methane into the
810 Hudson Canyon at the edge of methane clathrate hydrate stability. Geophysical Research Letters, in review
811 Westbrook GK, Thatcher KE, Rohling EJ, Piotrowski AM, Pälike H, Osborne AH, Nisbet EG, Minshull TA,
812 Lanoisellé M, James RH (2009) Escape of methane gas from the seabed along the West Spitsbergen continental
813 margin. Geophys Res Lett 36
814 Yamanaka T, Mizota C, Fujiwara Y, Chiba H, Hashimoto J, Gamo T, Okudaira T (2003) Sulphur-isotopic
815 composition of the deep-sea mussel Bathymodiolus marisindicus from currently active hydrothermal vents in the
816 Indian Ocean. J. Mar. Biol. Assoc. U. K. 83:841-848
817
818

**Tables**

| | Sediment | | Cement | | Groundmass | |
|---|---|---|---|---|---|---|
| | Norfolk | Baltimore Canyon | Norfolk | Baltimore Canyon | Norfolk | Baltimore Canyon |
| Mineral | - | - | Aragonite | Aragonite | Aragonite | Aragonite |
| $\%CaCO_3$ | 13.9±6.5 | 3.3 | 97.2 | 85.1 | 72.5 | 47.6 |
| $\%C_{org}$ | 3.7±1.4 | 0.64±0.14 | 0.16 | 0.28 | 0.27 | 0.39 |
| $\delta^{13}C$ (‰) | -31.9±9.0 | -23.4±3.0 | -47.3±0.16 | -49.2±0.21 | -44.3±0.07 | -47.7±0.92 |
| $\delta^{18}O$ (‰) | - | - | 3.84±0.07 | 4.35±0.06 | 3.78±0.03 | 3.54±0.04 |
| $^{87}Sr/^{86}Sr$ | - | - | 0.70917 | 0.70918 | 0.70920 | 0.70924 |

**Table 1**
Mineralogy (dominant carbonate phase), stable isotope, and percent calcium carbonate and organic carbon of authigenic carbonate cement and groundmass and sediment collected at the Norfolk and Baltimore canyons seep sites. Average values reported ±1 standard deviation.

| | Mussel Carbonate Shell | | Mussel Periostracum | Seawater | |
|---|---|---|---|---|---|
| | Norfolk | Baltimore Canyon | Norfolk | Norfolk | Baltimore Canyon |
| $\delta^{13}C$ (‰) | -2.59±1.68 (-7.10±3.20) | -6.84±1.97 | -56.99±12.8 | 0.90±0.06 | - |
| min | -6.53 (-16.74) | -10.91 | -70.66 | 0.86 | |
| max | 0.19 (-3.34) | -3.39 | -29.92 | 0.94 | |
| $\delta^{18}O$ (‰) | 3.71±0.25 (3.82±0.39) | 2.57±0.28 | - | 0.34±0.1 | 0.53±0.1 |
| min | 3.11 (3.46) | 2.06 | | | |
| max | 4.19 (5.13) | 3.59 | | | |
| $^{87}Sr/^{86}Sr$ | 0.70920 | - | - | 0.70917 | - |
| min | 0.70918 | | | 0.70915 | |
| max | 0.70921 | | | 0.70920 | |

**Table 2**
Geochemical composition of the *Bathymodiolus* sp. shell carbonate and periostracum material and seawater for carbon (±0.04‰), oxygen (±0.06‰), and strontium isotope ratios (±0.00002) for samples collected only at Norfolk. Average and standard deviations are reported. Ranges of values are also reported as minimum and maximum values; values in parenthesis are for dead specimens collected at Norfolk.

| | Gill | | Periostracum | | Sediment | |
|---|---|---|---|---|---|---|
| | Norfolk Seep | Baltimore Canyon | Norfolk Seep | Norfolk Seep | Norfolk Seep | Baltimore Canyon |
| Average (±σ) | 16.58±3.37 | 14.38±5.15 | 16.63±4.01 | 13.89±1.24 | 5.53±2.16 | 2.42±3.62 |
| Range | 8.65-21.55 | -4.07-18.13 | 8.82-22.65 | 13.01-14.77 | 2.98-8.20 | -2.62-6.30 |
| n | 23 | 20 | 28 | 2 | 4 | 5 |

Table 3
Sulfur isotope ($\delta^{34}S$; ‰) mussel gill and periostracum from *Bathymodiolus* sp. specimens collected at the Norfolk and Baltimore Canyon seep sites and adjacent seep sediment. The average, 1 standard deviation, and ranges of $\delta^{34}S$ values are reported.

| Station no. | Sample ID | Seep Field Site | Sample type | Fm | ±Fm Err | Age | Age Err | $\Delta^{14}C$ (‰) | $\pm\Delta^{14}C$ Err |
|---|---|---|---|---|---|---|---|---|---|
| RB-13-ROV-682 | RB-13-682-1 | Norfolk Canyon | authigenic carbonate-groundmass | 0.1136 | 0.0010 | 17480 | 80 | -887.3 | 1.0 |
| RB-13-ROV-682 | RB-13-682-2 | Norfolk Canyon | authigenic carbonate -cement | 0.1046 | 0.0010 | 18140 | 80 | -896.2 | 1.0 |
| RB-13-ROV-682 | RB-13-682-3 | Norfolk Canyon | authigenic carbonate -cement | 0.1175 | 0.0010 | 17200 | 80 | -883.4 | 1.0 |
| RB-13-ROV-682 | RB-13-682-4 | Norfolk Canyon | authigenic carbonate -cement | 0.0925 | 0.0010 | 19120 | 90 | -908.2 | 1.0 |
| RB-13-ROV-682 | RB-13-682-5 | Norfolk Canyon | shell in authigenic carbonate | 0.6094 | 0.0013 | 3980 | 20 | -395.3 | 1.3 |
| RB-13-ROV-682 | RB-13-682-6 | Norfolk Canyon | shell in authigenic carbonate | 0.6112 | 0.0013 | 3955 | 20 | -393.5 | 1.3 |
| NF-12-ROV-14 | NF-12-14-1 | Baltimore Canyon | authigenic carbonate-groundmass | 0.0670 | 0.0010 | 21710 | 130 | -933.5 | 1.0 |
| NF-12-ROV-14 | NF-12-14-2 | Baltimore Canyon | authigenic carbonate -cement | 0.0414 | 0.0010 | 25570 | 210 | -958.9 | 1.0 |
| NF-12-ROV-14 | NF-12-14-3 | Baltimore Canyon | authigenic carbonate -cement | 0.2617 | 0.0011 | 10770 | 35 | -740.3 | 1.1 |
| RB-13-ROV-689 | RB-13-ROV-689-M6 | Baltimore Canyon | mussel shell (alive) | 0.8782 | 0.0017 | 1045 | 20 | -128.6 | 1.7 |
| RB-13-ROV-689 | RB-13-ROV-689-M6 (rep) | Baltimore Canyon | mussel shell (alive) | 0.8747 | 0.0017 | 1075 | 20 | -132.0 | 1.7 |
| RB-13-ROV-689 | RB-13-ROV-689-M10 | Baltimore Canyon | mussel shell (alive) | 0.7859 | 0.0015 | 1935 | 20 | -220.2 | 1.5 |
| RB-13-ROV-687 | RB-13-ROV-687 | Norfolk Canyon | mussel shell (dead) | 0.8114 | 0.0016 | 1680 | 20 | -194.9 | 1.6 |
| RB-13-ROV-687 | RB-13-ROV-687 (rep) | Norfolk Canyon | mussel shell (dead) | 0.8078 | 0.0017 | 1715 | 20 | -198.5 | 1.7 |
| RB-13-ROV-683 | RB-13-ROV-683-Q16A | Norfolk Canyon | mussel shell (dead) | 0.7802 | 0.0015 | 1995 | 20 | -225.8 | 1.5 |
| RB-13-ROV-682 | RB-13-ROV-682-MQ9 | Norfolk Canyon | mussel shell (dead) | 0.8558 | 0.0021 | 1250 | 20 | -150.8 | 2.1 |
| RB-13-ROV-682 | RB-13-ROV-682- MQ8 | Norfolk Canyon | mussel shell (dead) | 0.9094 | 0.0017 | 765 | 15 | -97.6 | 1.7 |
| RB-13-ROV-682 | RB-13-ROV-682 | Norfolk Canyon | mussel shell (dead) | 0.8667 | 0.0018 | 1150 | 20 | -140.0 | 1.8 |
| RB-13-ROV-682 | RB-13-ROV-682 | Norfolk Canyon | mussel shell (dead) | 0.8632 | 0.0021 | 1180 | 20 | -143.5 | 2.1 |
| RB-13-ROV-682 | RB-13-ROV-682 10% HCl* | Norfolk Canyon | mussel shell (dead) | 0.8622 | 0.0018 | 1190 | 20 | -144.5 | 1.8 |
| RB-13-ROV-682 | RB-13-ROV-682 10% HCl* | Norfolk Canyon | mussel shell (dead) | 0.8624 | 0.0018 | 1190 | 20 | -144.2 | 1.8 |
| RB-13-ROV-683 | RB-13-ROV-683-M3 | Norfolk Canyon | mussel shell (alive) | 0.8937 | 0.0017 | 905 | 20 | -113.2 | 1.7 |
| RB-13-ROV-683 | RB-13-ROV-683-M17 | Norfolk Canyon | mussel shell (alive) | 0.8898 | 0.0018 | 940 | 20 | -117.1 | 1.8 |
| RB-13-ROV-683 | RB-13-ROV-683-49 | Norfolk Canyon | seawater | 0.9837 | 0.0037 | 130 | 30 | -23.7 | 1.7 |
| RB-13-ROV-682 | RB-13-ROV-682-2 | Norfolk Canyon | seawater | 0.9829 | 0.0027 | 140 | 20 | -24.6 | 1.8 |

**Table 4**

Summary data results for radiocarbon analysis including ROV station number (Station no.), sample identification (Sample ID), laboratory identification number (Lab ID), seep field, sample type, fraction modern (Fm) relative to standard, fraction modern error, $^{14}C$ age, $^{14}C$ age error, $\Delta^{14}C$ value as defined in Stuiver and Polach (1977), and $\Delta^{14}C$ error. Fraction Modern (Fm) is a measurement

of the deviation of the $^{14}C/^{12}C$ ratio of a sample from "Modern." Modern is defined as 95% of the radiocarbon concentration (in AD 1950) of NBS Oxalic Acid I normalized to $\delta^{13}C_{VPDB}$=-19 per mil (Olsson 1970). *Samples pretreated with 10% HCl

| | | | | MEASURED | | | | CORRECTED | | | | |
|---|---|---|---|---|---|---|---|---|---|---|---|---|
| Sample Name | Wt (mg) | U (ppm) | 232Th (ppb) | $^{230}Th/^{232}Th$ $AR_{(a)}$ | $^{232}Th/^{238}U$ $AR_{(a)}$ | $^{230}Th/^{238}U$ $AR_{(a)}$ | $^{234}U/^{238}U$ $AR_{(a)}$ | $^{230}Th/^{238}U$ $AR_{(b)}$ | $^{234}U/^{238}U$ $AR_{(b)}$ | Rho 08-48 | Age (ka) | $^{234}U/^{238}Ui$ AR |
| *Carbonate samples* | | | | | | | | | | | | |
| Norfolk Canyon | | | | | | | | | | | | |
| RB-13-682 D | 8.8 | 3.223 ± 0.037 | 271 ± 3 | 2.413 ± 0.015 | 0.02766 ± 0.00002 | 0.0668 ± 0.0004 | 1.143 ± 0.001 | 0.027 ± 0.015 | 1.146 ± 0.005 | 0.236 | 2.6 ± 1.4 | 1.147 ± 0.006 |
| RB-13-682 E | 16.6 | 3.393 ± 0.021 | 261 ± 2 | 2.776 ± 0.012 | 0.02524 ± 0.00002 | 0.0701 ± 0.0003 | 1.143 ± 0.001 | 0.034 ± 0.013 | 1.146 ± 0.005 | 0.238 | 3.3 ± 1.3 | 1.147 ± 0.005 |
| RB-13-682 F | 12.3 | 3.427 ± 0.028 | 65 ± 1 | 3.844 ± 0.028 | 0.00623 ± 0.00001 | 0.0240 ± 0.0002 | 1.145 ± 0.001 | 0.015 ± 0.003 | 1.145 ± 0.002 | 0.149 | 1.4 ± 0.3 | 1.146 ± 0.002 |
| RB-13-682 G | 17.2 | 4.209 ± 0.025 | 209 ± 1 | 2.218 ± 0.012 | 0.01632 ± 0.00001 | 0.0362 ± 0.0002 | 1.143 ± 0.001 | 0.012 ± 0.009 | 1.145 ± 0.003 | 0.223 | 1.2 ± 0.8 | 1.145 ± 0.003 |
| RB-13-682 H | 14.2 | 3.670± 0.026 | 160 ± 1 | 2.231 ± 0.014 | 0.01435 ± 0.00001 | 0.0320 ± 0.0002 | 1.143 ± 0.001 | 0.011 ± 0.008 | 1.145 ± 0.003 | 0.218 | 1.0 ± 0.7 | 1.145 ± 0.003 |
| Baltimore Canyon | | | | | | | | | | | | |
| NF12-14 D | 13.0 | 3.894 ± 0.030 | 344 ± 3 | 5.835 ± 0.017 | 0.02899 ± 0.00002 | 0.1692 ± 0.0006 | 1.139 ± 0.001 | 0.145 ± 0.009 | 1.143 ± 0.005 | 0.301 | 14.8 ± 1.0 | 1.149 ± 0.006 |
| NF12-14 E | 4.7 | 4.073 ± 0.087 | 241 ± 5 | 8.585 ± 0.036 | 0.01941 ± 0.00001 | 0.1667 ± 0.0008 | 1.140 ± 0.002 | 0.151 ± 0.006 | 1.142 ± 0.004 | 0.283 | 15.4 ± 0.6 | 1.148 ± 0.004 |
| NF12-14 F | 6.4 | 4.592 ± 0.072 | 268 ± 4 | 8.342 ± 0.029 | 0.01916 ± 0.00001 | 0.1598± 0.0006 | 1.141 ± 0.001 | 0.144 ± 0.006 | 1.143 ± 0.004 | 0.283 | 14.7 ± 0.6 | 1.149 ± 0.004 |
| NF12-14 G | 4.1 | 4.588 ± 0.112 | 433 ± 11 | 5.682 ± 0.023 | 0.03103 ± 0.00002 | 0.1763 ± 0.0008 | 1.139 ± 0.002 | 0.151 ± 0.010 | 1.142 ± 0.006 | 0.299 | 15.4 ± 1.0 | 1.148 ± 0.006 |
| NF12-14 H | 6.9 | 4.110 ± 0.060 | 586 ± 9 | 4.087 ± 0.013 | 0.04681 ± 0.00002 | 0.1913 ± 0.0007 | 1.136 ± 0.002 | 0.153 ± 0.015 | 1.141 ± 0.009 | 0.311 | 15.7 ± 1.6 | 1.147 ± 0.009 |
| *Detritus samples* | | | | | | | | | | | | |
| Norfolk Canyon | | | | | | | | | | | | |
| RB13-D682-PC03 A | 77.1 | 1.959 ± 0.003 | 8167 ± 14 | 1.509 ± 0.003 | 1.36986 ± 0.00113 | 2.0674 ± 0.0052 | 0.989 ± 0.001 | | | | | |
| RB13-D682-PC03 B | 142.9 | 1.764 ± 0.002 | 7403 ± 12 | 1.492 ± 0.003 | 1.37909 ± 0.00172 | 2.0576 ± 0.0057 | 0.989 ± 0.001 | | | | | |
| RB13-D682-PC03 C | 134.6 | 1.858 ± 0.002 | 7865 ± 27 | 1.467 ± 0.007 | 1.39116 ± 0.00451 | 2.0403 ± 0.0089 | 0.990 ± 0.001 | | | | | |
| RB13-D682-PC04 A | 75.6 | 2.165 ± 0.003 | 7166 ± 12 | 1.588 ± 0.003 | 1.08744 ± 0.00082 | 1.7272 ± 0.0042 | 1.012 ± 0.001 | | | | | |
| RB13-D682-PC04 B | 82.1 | 2.486 ± 0.003 | 8597 ± 15 | 1.556 ± 0.004 | 1.13645 ± 0.00125 | 1.7682 ± 0.0050 | 1.008 ± 0.001 | | | | | |
| Baltimore Canyon | | | | | | | | | | | | |
| NF12-14 1 | 11.1 | 2.756 ± 0.025 | 18081 ± 164 | 0.680 ± 0.001 | 2.15602 ± 0.00178 | 1.4664 ± 0.0037 | 0.993 ± 0.001 | | | | | |
| NF12-14 2 | 15.0 | 1.990 ± 0.013 | 8551 ± 57 | 0.936 ± 0.002 | 1.41179 ± 0.00069 | 1.3208 ± 0.0034 | 0.995 ± 0.001 | | | | | |
| NF12-071-185 B | 126.5 | 1.118 ± 0.001 | 4119 ± 9 | 1.118 ± 0.005 | 1.21060± 0.00220 | 1.3530 ± 0.0058 | 1.000 ± 0.001 | | | | | |
| NF12-071-185 C | 107.6 | 1.237 ± 0.001 | 5799 ± 8 | 0.843 ± 0.002 | 1.54106 ± 0.00123 | 1.2984 ± 0.0035 | 0.994 ± 0.001 | | | | | |

**Table 5**

Summary data for measured U-Th data for authigenic carbonate samples and activity ratios (AR) used for age calculation and U-Th ages. All activity ratios were calculated using $\lambda^{230}$=9.17050E-6, $\lambda^{234}$=2.82206E-6 (Cheng et al., 2013), $\lambda^{232}$=4.93343E-11 (Holden et al., 1990), $\lambda^{238}$=1.55125E-10 (Jaffey et al., 1971), (a) - Activity ratios corrected for hydride formation, tailing, fractionation, SEM-Faraday yield, and tracer isotopic composition, (b) Corrected using average measured detrital U and Th isotopic compositions for the Norfolk Canyon (($^{232}$Th/$^{238}$U) = 1.38, ($^{230}$Th/$^{238}$U) = 2.05 and ($^{234}$U/$^{238}$U) = 0.99, n=3) and Baltimore Canyon (($^{232}$Th/$^{238}$U) = 1.39, ($^{230}$Th/$^{238}$U) = 1.32 and ($^{234}$U/$^{238}$U) = 1.00, n=3) sites with all uncertainties arbitrarily set at ± 25% (see main text section 3.5 for details)

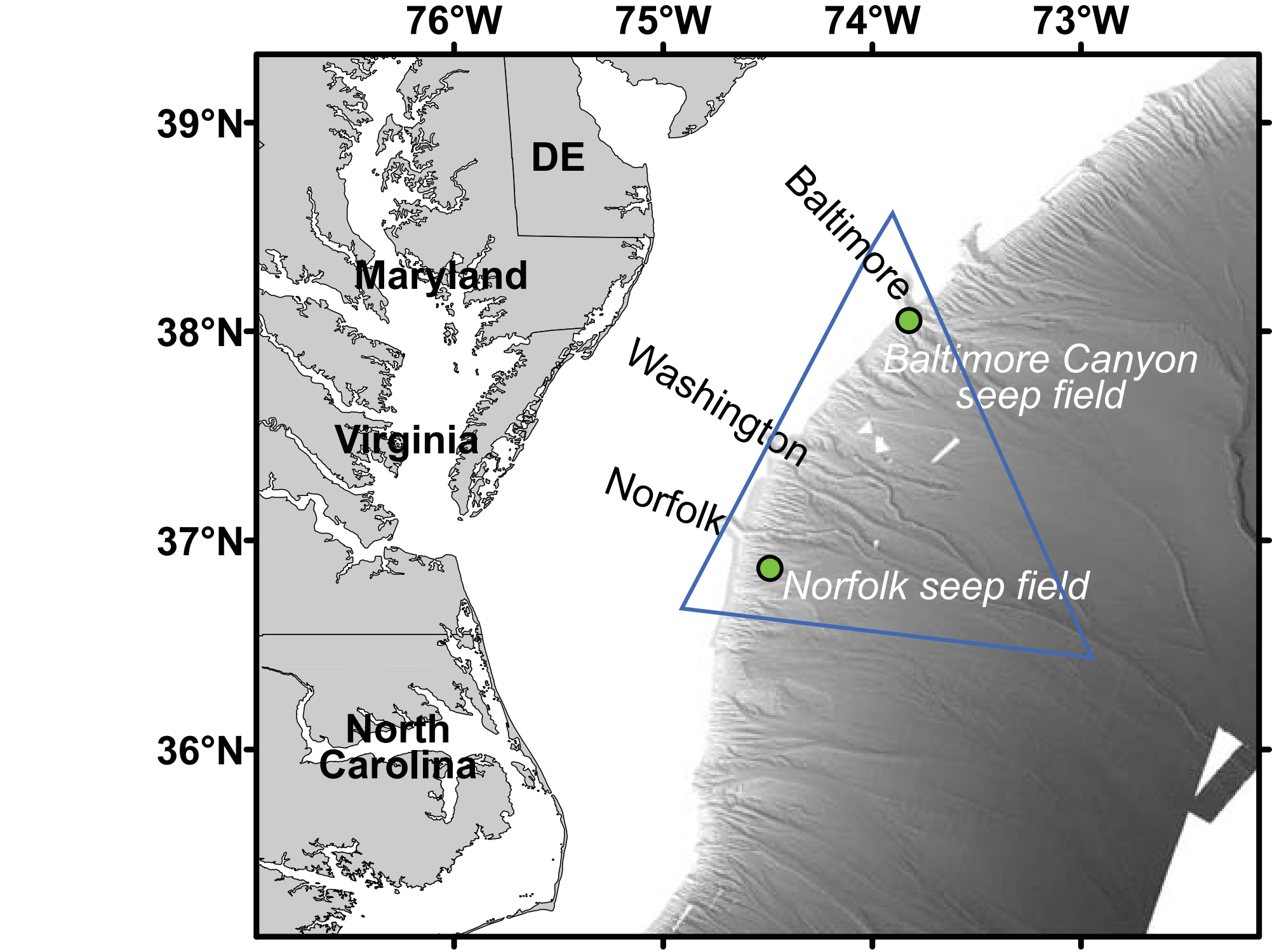


Figure 1, Prouty et al.

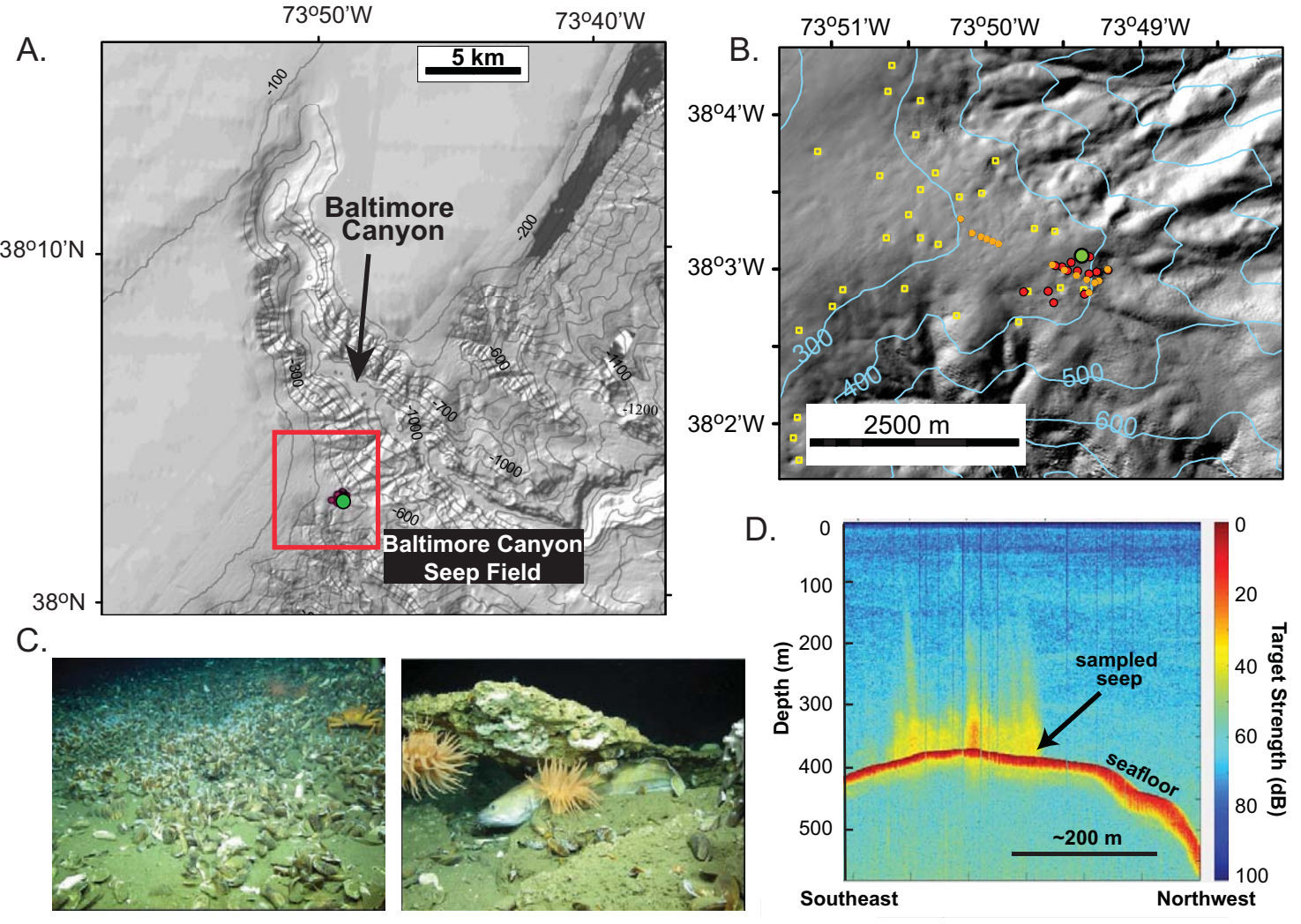


Figure 2, Prouty et al.

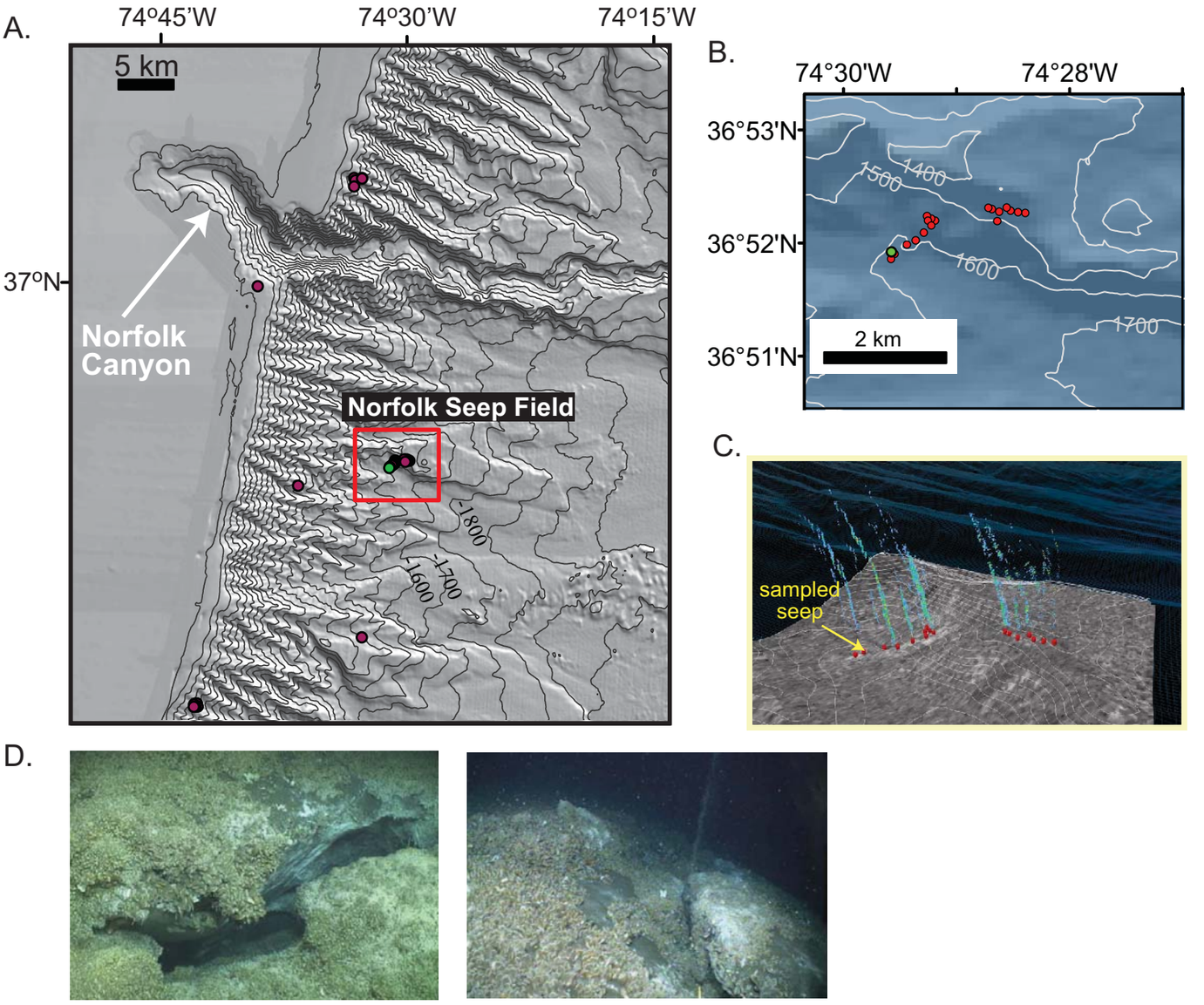


Figure 3. Prouty et al.

Figure 4, Prouty et al.

Norfolk (RB-2013-682)

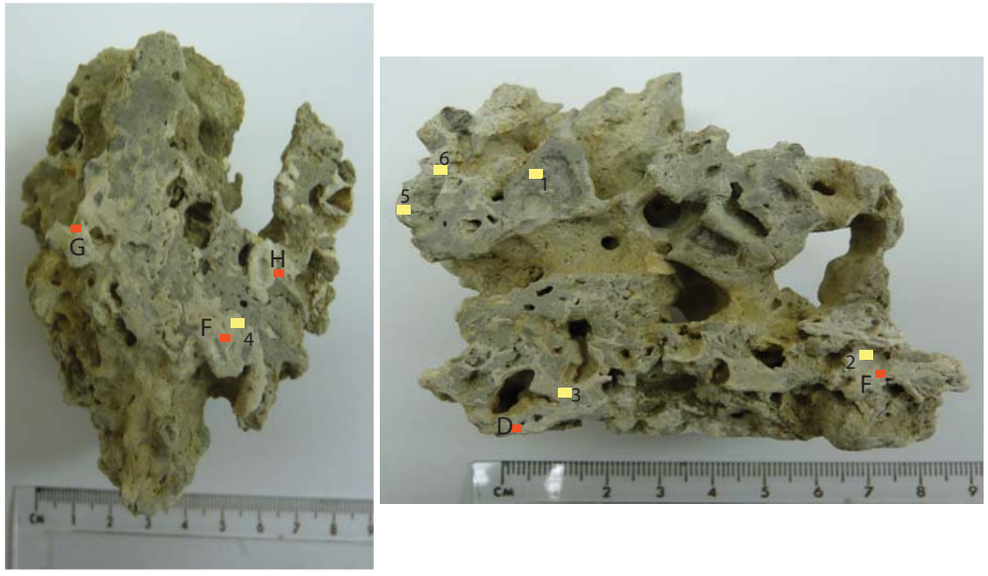


Baltimore Canyon (NF-2012-14)

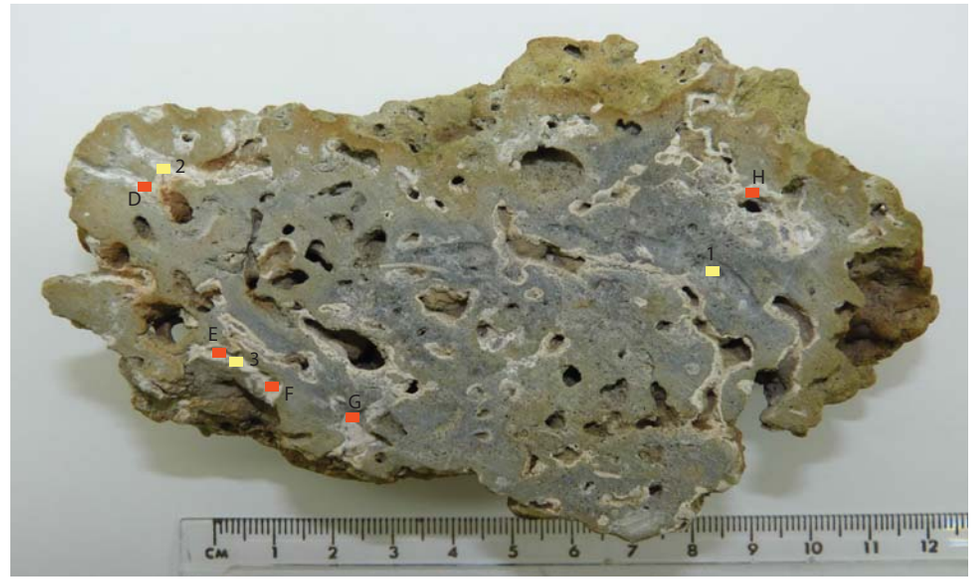


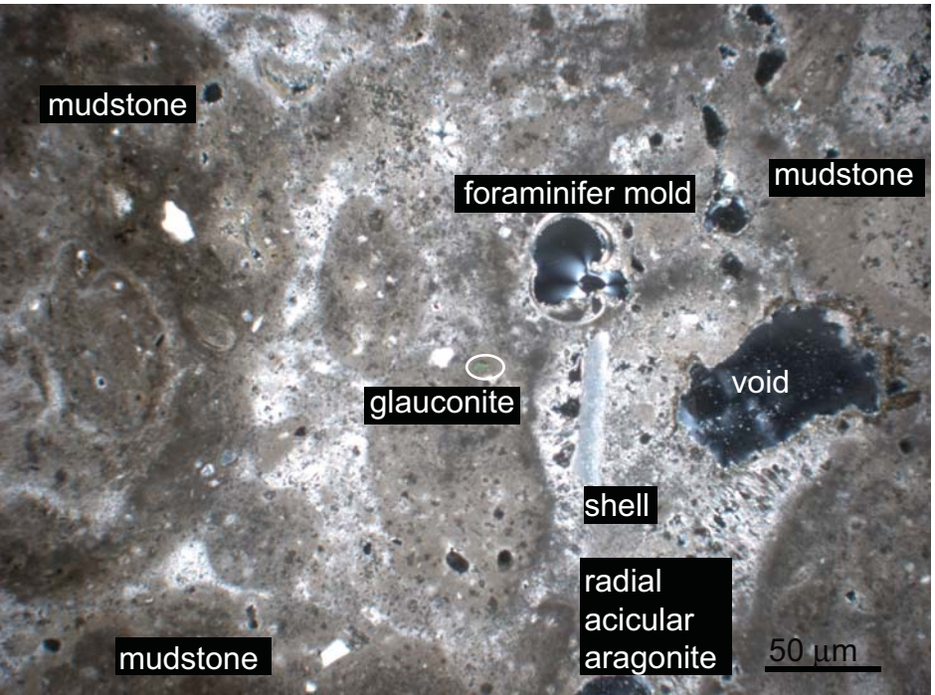


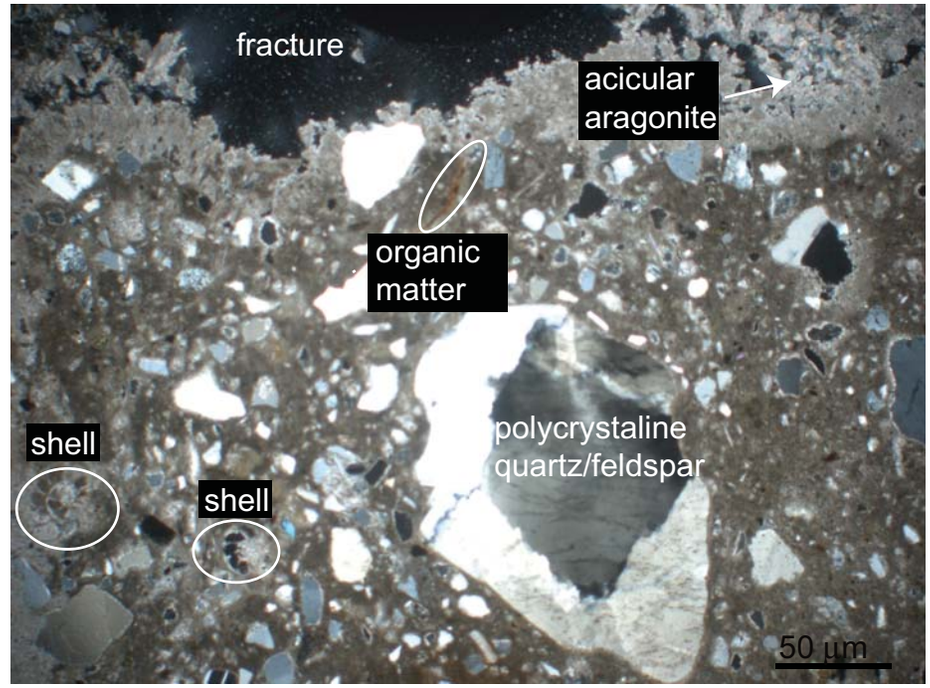

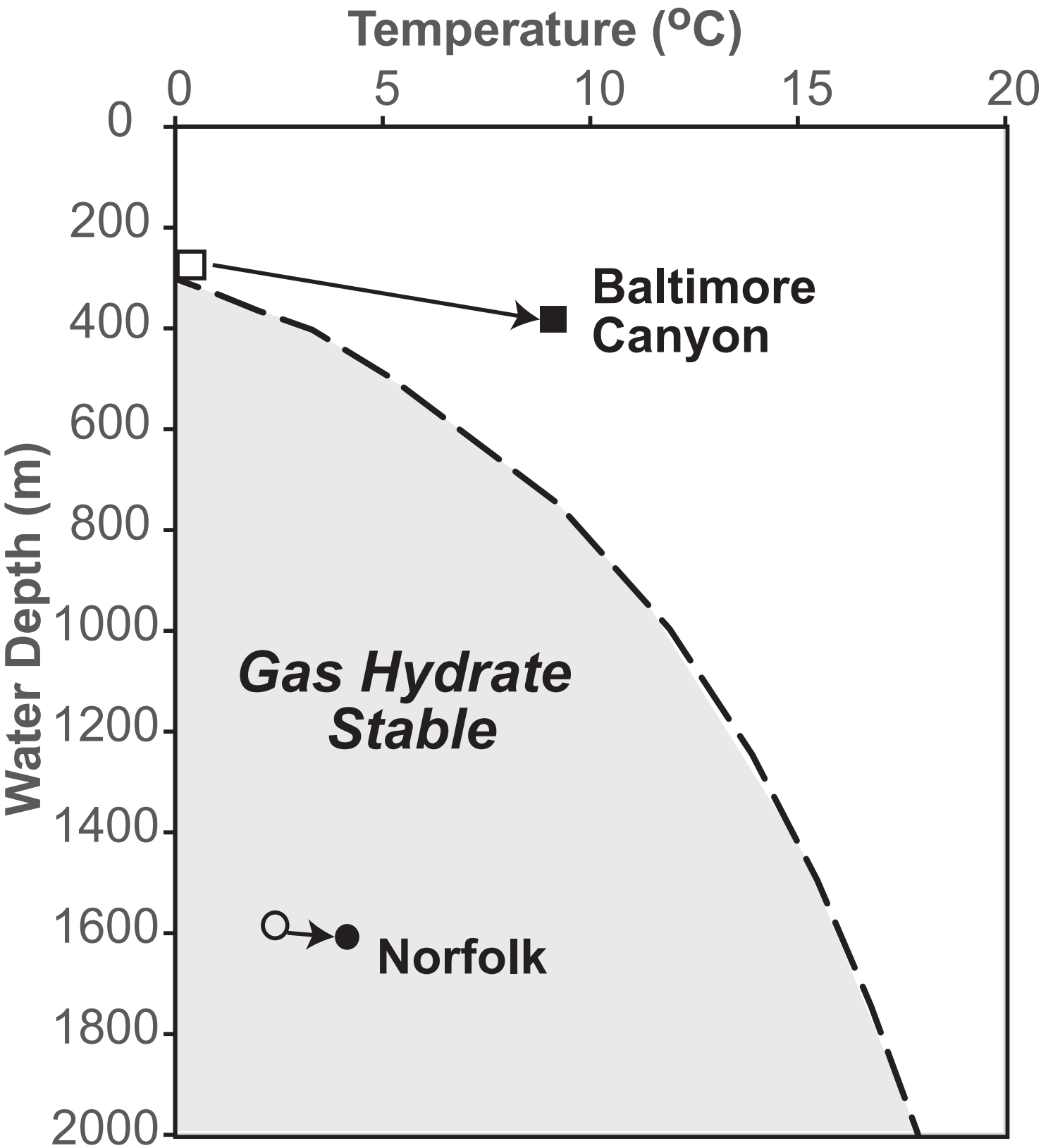


Figure 5, Prouty et al.

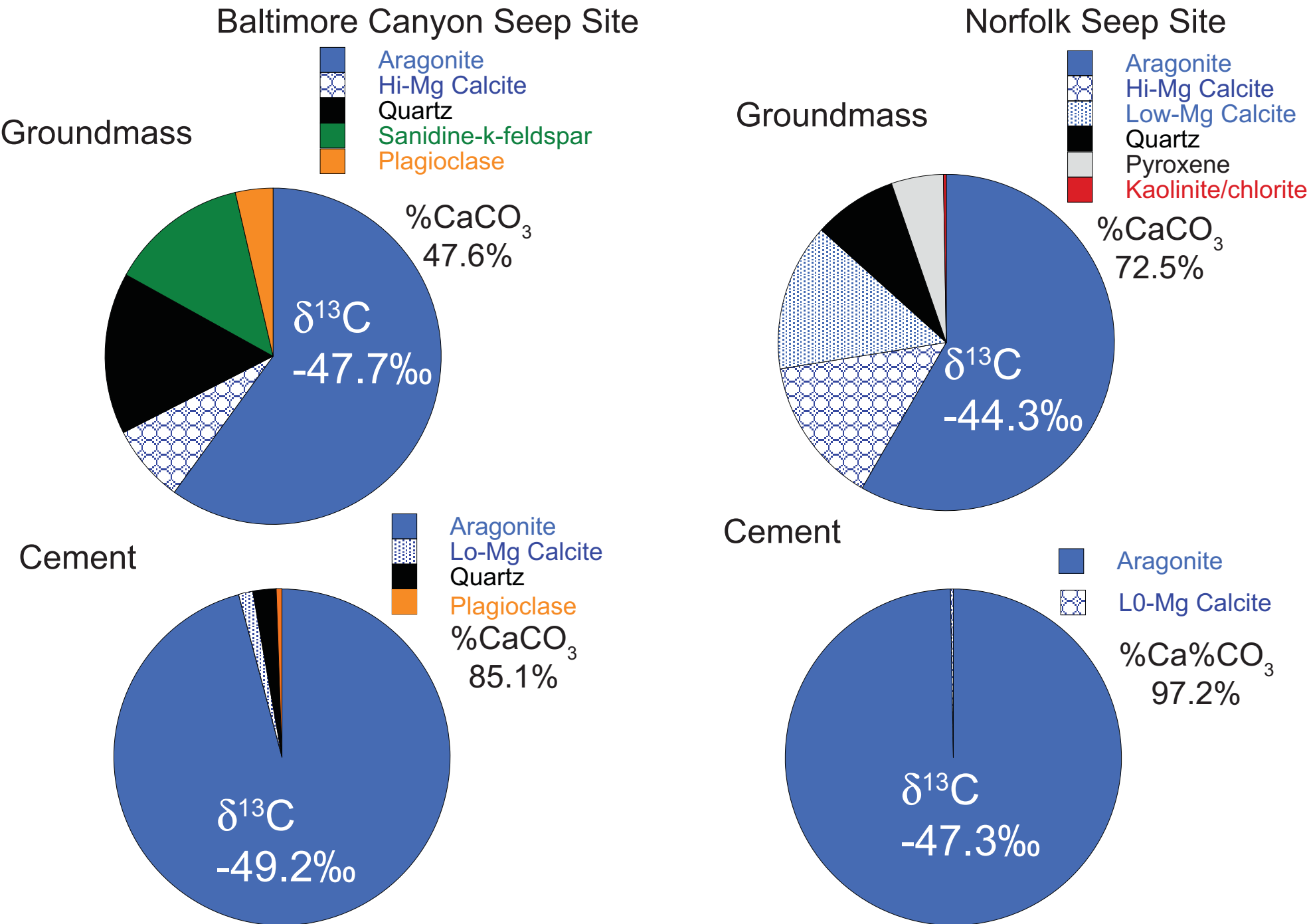
Baltimore Canyon Seep Site
Groundmass
Aragonite
Hi-Mg Calcite
Quartz
Sanidine-k-feldspar
Plagioclase
%CaCO3
47.6%
δ13C
-47.7‰
Cement
Aragonite
Lo-Mg Calcite
Quartz
Plagioclase
%CaCO3
85.1%
δ13C
-49.2‰
Norfolk Seep Site
Groundmass
Aragonite
Hi-Mg Calcite
Low-Mg Calcite
Quartz
Pyroxene
Kaolinite/chlorite
%CaCO3
72.5%
δ13C
-44.3‰
Cement
Aragonite
L0-Mg Calcite
%Ca%CO3
97.2%
δ13C
-47.3‰

Figure S2, Prouty et al.

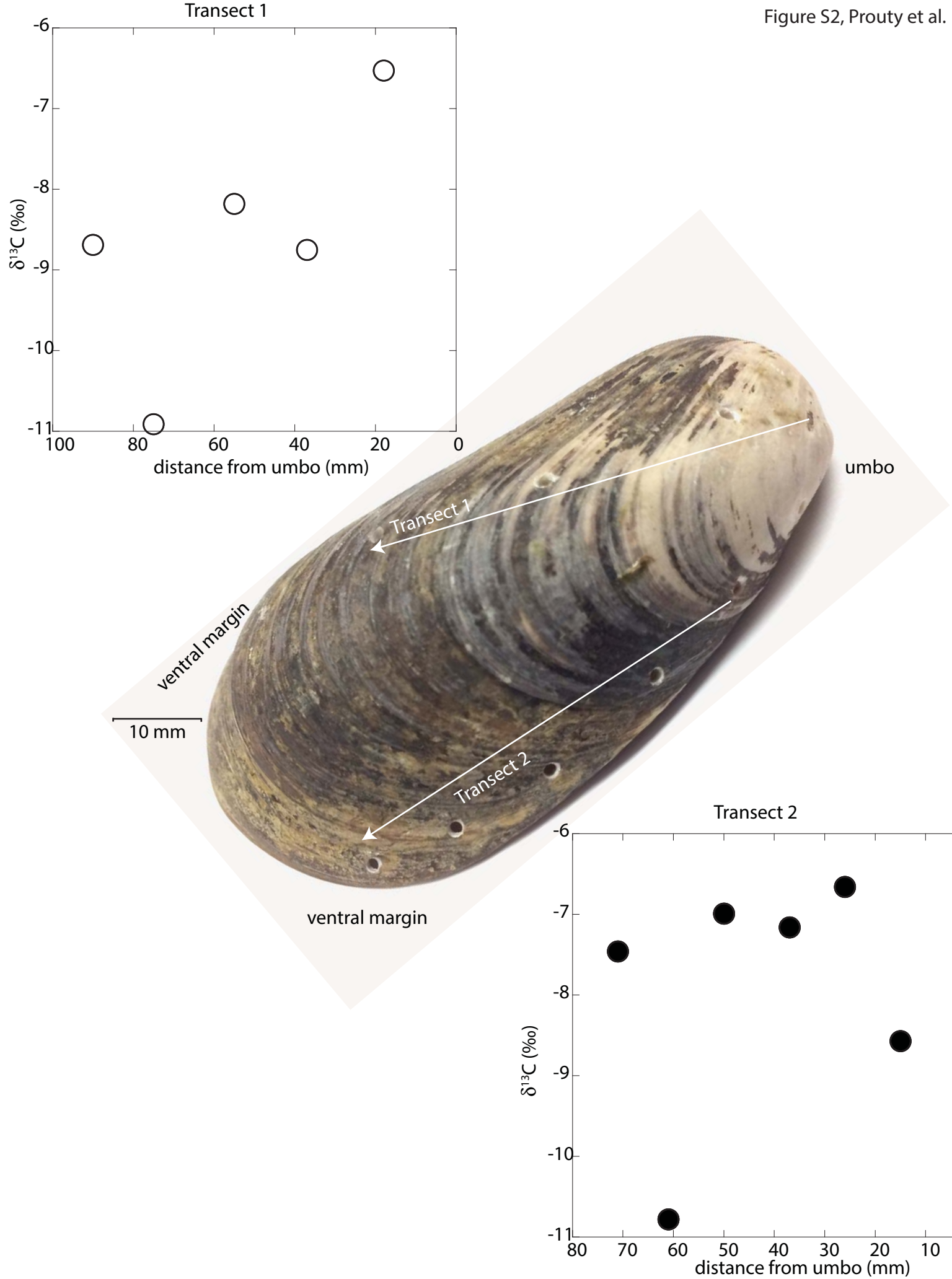

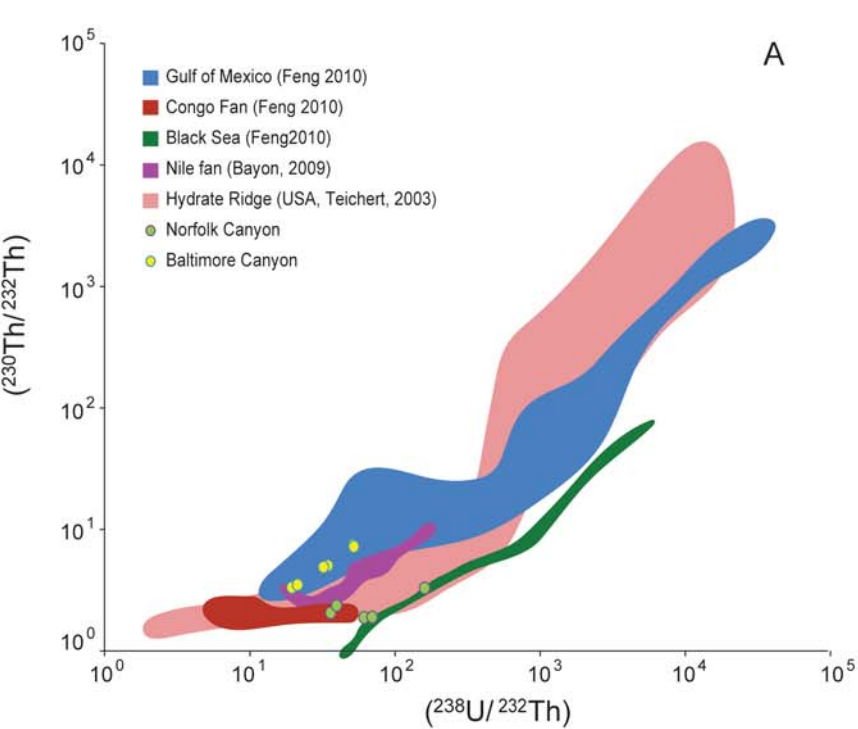
A
Gulf of Mexico (Feng 2010)
Congo Fan (Feng 2010)
Black Sea (Feng2010)
Nile fan (Bayon, 2009)
Hydrate Ridge (USA, Teichert, 2003)
Norfolk Canyon
Baltimore Canyon
$(^{230}Th/^{232}Th)$
$(^{238}U/^{232}Th)$
$10^0$
$10^1$
$10^2$
$10^3$
$10^4$
$10^5$

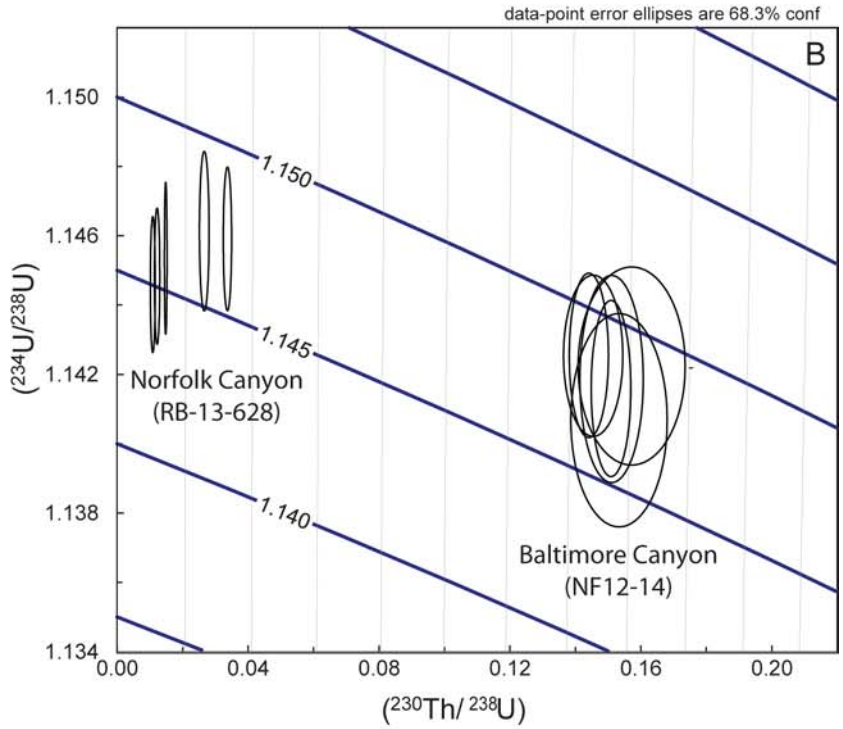
data-point error ellipses are 68.3% conf
B
1.150
1.146
1.142
1.138
1.134
1.150
1.145
1.140
Norfolk Canyon
(RB-13-628)
Baltimore Canyon
(NF12-14)
$(^{234}U/^{238}U)$
$(^{230}Th/^{238}U)$
0.00
0.04
0.08
0.12
0.16
0.20

**Insights into methane dynamics from analysis of authigenic carbonates and chemosynthetic mussels at newly-discovered Atlantic Margin seeps**

Prouty et al.,

**Supplementary Material**

## 1. U-Th analytical protocol

Analytical protocols for U-Th dating were aimed at ensuring: (i) complete dissolution of the detrital material incorporated into the authigenic carbonates, and (ii) oxidation of organic material liable to produce isobaric interferences during measurements of Th isotope ratios (Shen et al. 2002). Carbonate samples were dissolved in 8M $HNO_3$, spiked with a mixed $^{229}$Th-$^{236}$U tracer, left to equilibrate overnight, and dried. All evaporation steps took place in a closed EvapoClean device, in order to minimise cross-contamination and reduce fall-in blanks. To ensure total dissolution of detrital mineral, samples were refluxed in a mixture of 11 M $HClO_4$: 29 M HF : 16 M $HNO_3$ (1:2:2.5), for 1-7 days, using ~50 µl HF per mg of material. Following evaporation to dryness, samples went through two overnight oxidation steps in 2 ml 16M $HNO_3$ and 0.2 ml 30% $H_2O_2$. Pre-concentration of U and Th through Fe co-precipitation and initial separation of U and Th on 0.6 ml columns using AG-1 x 8 anion exchange resin followed (Edwards et al. 1987). Th fractions were further purified using a second pass through AG-1 x 8 resin, and were filtered using 0.22 µm syringe filters to remove resin particles. Both U and Th fractions were oxidised twice in 2 ml 16M $HNO_3$ and 0.2 ml 30% $H_2O_2$, and dissolved in 1 ml 0.1M HCl and 0.035 M HF. Prior to mass spectrometry, all samples were filtered to remove particles originating from the FEP beakers used for sample preparation.

Isotope ratio measurements were made on a Thermo Neptune Plus multi-collector ICP-MS, with samples introduced via an Aridus II desolvating nebuliser. U and Th were measured separately, using an X skimmer cone coupled with normal and Jet sample cones respectively. Measurements were made using static multicollector data collection protocols with $^{234}$U and $^{230}$Th measured on an axial

secondary electron multiplier (SEM) and the remaining isotopes ($^{233}$U, $^{235}$U, $^{236}$U, $^{238}$U and $^{229}$Th, $^{232}$Th respectively) measured on Faraday cups equipped with $10^{11}$ Ω resistors. SEM/Faraday gain and exponential mass fractionation were monitored and corrected for via a sample-standard bracketing approach using CRM 112a U, and mixed CRM 112a U + IRMM 3636 spike for U, and an in-house $^{229}$Th-$^{230}$Th-$^{232}$Th reference solution calibrated against CRM 112a for Th. Hydride formation and tailing were monitored at the beginning of each analytical session, with measurements made at mass 237 and 239 while aspirating an unspiked CRM 112a solution, and were corrected off-line. Laboratory blanks ($2.3 \times 10^{-11}$g $^{238}$U, $6.3 \times 10^{-12}$ $^{232}$Th) were negligible compared to sample size for all isotopes except $^{230}$Th, for which procedural blanks amounted to 2.6 ± 0.7 fg resulting in sample/blank ratios of 5-29 (with a mean of 20) for the analyzed authigenic carbonate samples. Consequently, a blank correction was applied by subtracting the mean $^{230}$Th signal of three un-spiked total procedural blanks from each analyzed sample.

## 2. Calculated detritus U-Th ratios at Norfolk Canyon and Baltimore Canyon

At Norfolk Canyon, two of the five analysed detritus samples were considered unsuitable for use as the basis of a detrital correction, as they exhibited ($^{234}$U/$^{238}$U) values above 1, which indicates the presence of some proportion of authigenic and/or biogenic carbonate of unknown age (but too young to have reached secular equilibrium). The remaining three samples gave mean activity ratios of ($^{232}$Th/$^{238}$U)=1.380 (± 1.55%), ($^{230}$Th/$^{238}$U) = 2.055 (±1.33%) and ($^{234}$U/$^{238}$U) = 0.99 (±0.32%). Given that mean values are based on only three analyses, they are unlikely to encompass the full spectrum of carbonate-free detrital U and Th compositions available at the Norfolk Canyon site. Consequently, in order to ensure that corrected age uncertainties remain at a realistic level, the detrital correction applied at Norfolk Canyon is based on the nominal mean values of detrital activity ratios, with uncertainties set at ± 25%. At Baltimore Canyon, all four of the analysed detrital samples appear to be free of young carbonate material on the basis of their ($^{234}$U/$^{238}$U) values. One sample exhibited an atomic Th/U ratio of 6, significantly higher than other detritus samples which clustered around 3-4 at both sites, possibly due to the presence of Th-rich minerals, such as monazite, or

detrital grains with Fe-oxide coating, which preferentially incorporates Th. The remaining three samples gave mean activity ratios of ($^{232}Th/^{238}U$)=1.387 (± 24%), ($^{230}Th/^{238}U$) = 1.324 (±4.14%) and ($^{234}U/^{238}U$) = 0.996 (±0.61%). To ensure consistency with the approach used at Norfolk Canyon, the detrital correction used for the Baltimore Canyon carbonate samples was also based on mean nominal activity ratios, and associated uncertainties of ± 25%.

References:

Edwards RL, Chen JH, Wasserburg GJ (1987) $^{238}U$-$^{234}U$-$^{230}Th$-$^{232}Th$ Systematics and the Precise Measurement of Time over the Past 500000 Years. Earth Planet. Sci. Lett. 81:175-192

Shen C-C, Lawrence Edwards R, Cheng H, Dorale JA, Thomas RB, Bradley Moran S, Weinstein SE, Edmonds HN (2002) Uranium and thorium isotopic and concentration measurements by magnetic sector inductively coupled plasma mass spectrometry. Chem Geol 185:165-178

**Figure S1**

Mineralogical composition of the groundmass and carbonate from the authigenic carbonates collected from the Norfolk seep (dive NF-2012-14) and Baltimore Canyon seep (dive RB-2013-682) sites based on X-ray diffraction (XRD). Semi-quantitative mineral percentages were determined by multiplying unique peak intensities for each mineral in a sample by intensity factors relative to quartz as 1. The products for all minerals in each sample were then summed to 100%. Stable carbon isotope ($\delta^{13}C$; ‰) and percent calcium carbonate ($CaCO_3$) are noted for the cement and groundmass.

**Figure S2**

Lifespan carbonate stable carbon isotope ($\delta^{13}C$) variability of a mussel collected alive from the Virginia seep field at 1457 m. Subsampling of shell for two transects from the umbo to the ventral margin.

**Figure S3**

A – Rosholt type diagram showing a comparison between U-Th data from this study and other occurrences of methane-related authigenic carbonates. The offset between data from Norfolk Canyon and Baltimore Canyon indicates that initial Th incorporated in the carbonate samples had different

($^{230}Th/^{232}Th$ ) signatures at the two localities, which is consistent with U-Th data from measured detritus samples. B – ($^{230}Th/^{238}U$) – ($^{234}U/^{238}U$) evolution diagram showing that carbonate samples crystallized from fluids with initial ($^{234}U/^{238}U$) similar to the 1.1466 mean moderns seawater value (Robinson et al., 2004).